Channel Modeling and Interference Rejection for CDMA Automatic Vehicle Monitoring Systems

by

Raymond Sihao Zheng

Thesis submitted to the Faculty of the
Virginia polytechnic Institute and State University
in partial fulfillment of the requirements for the degree of

MASTER OF SCIENCE

in

Electrical Engineering

APPROVED:

Dr. Jeffrey H. Reed, Chairman

Dr. Brian D. Woerner

Dr. Wayne Scales

Channel Modeling and Interference Rejection for CDMA Automatic Vehicle Monitoring Systems

by

Raymond S. Zheng
Committee Chairman: Jeffery H. Reed
Electrical Engineering
(ABSTRACT)

It is desirable to develop a universal digital receiver which is capable of operating with many different wireless communication systems. Time Dependent Adaptive Filter (TDAF) Processing represents an effective approach for CDMA interference rejection. This technique is especially appropriate at the mobile receiver where there is little prior knowledge of the spreading codes of the other users.

This thesis presents enhanced forms of the Time Dependent Adaptive Filter (TDAF), which is an optimal periodically time-varying adaptive filter. It is able to fully exploit the cyclostationarity and spectral correlation in certain DS-SS signals. It is shown how multiple AVM service providers can exist in adjacent channels within the ISM band. It is demonstrated that using the realistic channel models the TDAF can provide substantial improvement in interference rejection over the conventional correlation receiver. Computationally efficient TDAF structures have been also proposed to handle the case of different code repeat intervals for different systems.

Results of CDMA overlay system simulation have shown that TDAF processing can achieve tremendous gain in narrowband interference rejection compared to notch/matched filter processing. An input signal which has 45 dB narrowband interference-to-signal power ratio (J/S), the SIR of the TDAF processed output signal can be 20 dB, a 65 dB improvement. The use of TDAF processing and a spectral shaping filter can minimize the impact of adjacent channel interference. Even in an environment which has a 30 dB adjacent channel J/S, the SIR at output is demonstrate to be a 50 dB improvement. System performance shows little degradation by adjacent channel and narrowband interference.

Acknowledgments

To my academic advisor, Professor Jeffrey H. Reed, I would like to express my sincere appreciation for his guidance, his support, and the opportunity to perform this research. I also like to extend my gratitude to my committee members, Dr. Brian D. Woerner and Dr. W. Scales for countless discussions and suggestions throughout this research.

To sponsor of this project, Southwestern Bell Mobile System, I am deeply indebted for providing this research opportunity.

I am very grateful to every member of the Mobile and portable Radio Research who assisted me through this thesis. I would like to express my appreciation to Frank Cheng, Carl Dietrich, Francis Dominique, Anil Doradla, Jenny Frank, Rong He, Ashish Kaul, Young Kim, Jeff Laster, Nitin Mangalvedhe, Rias Muhamed, Paul Petrus, Sandip Sandhu, JiannAn Tsai, Annie Wade, Kathy Wolfe, Ning Yang, Kau Yao and many others in the lab. I would also like to express my appreciation and acknowledge to Dr. Theodore S. Rappaport for his leadership in this great research group.

I would like to thank my great family - my Mom, Dad, Grandma, Grandpa who I dearly miss for their endless support and understanding in these years. To my aunt and uncle, Mr. & Mrs. T.Z. Wang, I am deeply indebted for their insight, encouragement, and support.

Contents

List of Figures

List of Tables

Chapter 1

Overview of Automatic Vehicle Monitoring Systems

1.0 Introduction

In recent years, mobile communication products have experienced tremendous growth. The huge market has driven the industry to offer more new services, such as Automatic Vehicle Monitoring (AVM).

Currently, cellular networks cover every major highway in North America. Customers can use their cellular phones to call anyone or send data anywhere. At the same time, the Global Positioning System (GPS) uses its satellite systems to offer a position location message service. The idea behind AVM systems is to combine position and messaging service together with more new features. AVM systems can have substantially different forms; however, most AVM systems will offer the following features.

- Two-way communications: Transmitting of data or voice messages to and from vehicles.
- Position location: Tracking and reporting vehicle locations in real time.

- Vehicle security and emergency services: Enabling and disabling of vehicle security alarms and giving emergency roadside assistance with position notification.
- Navigation guides: providing customers with directions to destination by digital map databases, along with position location information.

There is a wide variety of potential applications for AVM systems, such as fleet management and traffic management. Fleet management can allow large transportation companies to direct their trucks more efficiently. Traffic management can be used to control and optimize traffic routes, perform automatic toll collection, and much more.

Several companies are in the process of developing and deploying AVM systems. The Federal Communications Commission (FCC) has indicated its intention to create rules which foster this creative use of the ISM band. In one recently proposed rule, the FCC proposed guidelines for offering AVM service within the 902-928 MHz ISM band. However, FCC part 15 devices are also operating in the 902-928 MHz ISM band. In order to coexist with narrowband users, Code Division Multiple Access (CDMA) modulation should be employed by AVM systems. In this way, CDMA based AVM systems could operate in the ISM band as co-primary users.

This research project aims to develop a receiver which implements nearly all functions with digital signal processing (DSP). The need for such a universal digital receiver is driven by the proliferation of wireless transmission standards. The programmable receiver can be used in many different communications systems. Alternatively, the receiver can

take advantage of future advances in communications technology by updating the software to make the receiver compatible with evolving communication standards.

Development of a universal digital receiver for AVM systems would greatly advance the acceptance of AVM systems. A single receiver could operate in conjunction with each of the competing AVM standards, making each standard more viable. In addition to improving compatibility, an all digital receiver can use of advanced DSP algorithms for interference mitigation.

1.1 Spectrum sharing

While agreement among different proposals can be found on many issues, spectrum sharing remains a significant point of contention. CDMA is a modulation and multiple access scheme based on spread spectrum (SS). Unlike Frequency Division Multiple Access (FDMA), in which signals are assigned narrowband frequency slots, and Time Division Multiple Access (TDMA), in which signals are assigned specific time slots, CDMA signals are modulated with a pseudo-random binary sequence which spreads the signal energy over a wideband. This technique allows a large number of CDMA signals to share the same spectrum. The signals are separated at the receiver using a correlator which multiplies a time-synchronized replica of the spreading code to remove the spreading code from the desired signal and reject other CDMA signals.

The capacity and overall quality of the CDMA systems are maximized through the use of power control. By controlling the transmit power of each mobile station, link quality is maintained and interference to other users is minimized with a minimum required signal-to-noise ratio. To achieve this, two power control loops can be used, the "open loop" and the "closed loop". Open loop power control is primarily used by the mobile station (MS). The MS transmit power is estimated directly from the MS receiver power. The purpose of the open loop is to provide rapid transmit power adjustment according to changes in received power from the cell.

Closed-loop power control is performed by the base station (BS). The BS measures the received signal energy per bit to noise density ratio, E_b/N_0 from each mobile unit and commands the mobile transmitter to adjust its power and maintain it at an adjustable threshold, which depends upon the frame error rate (FER) of the link. The purpose of the closed-loop power control is to provide corrections to the open loop estimates in order to maintain precise transmit power given a desired FER.

The design of CDMA networks requires methods that differ dramatically from the design of analog FM networks. One of the key factors is that geographical distribution of users has an influence on the coverage and capacity of CDMA networks. No matter which AVM system is used, power control for each user is very important for maximizing channel capacity.

If there is more than one system using the same frequency band, it would be extremely difficult to have power control among users from different systems. Without good power control, the overall system capacity can suffer severe degradation. Also, different systems would need to coordinate signature sequences assigned to each user. Therefore, sharing the same frequency band does not appear to be practical.

An alternative is to place AVM systems in adjacent bands. It is possible to locate the mainlobe of one system's spectrum over a sidelobe of a second system's spectrum. This would allow efficient spectrum usage and mitigate the interference between systems. To realize a partial overlay system, spectral shaping techniques must be employed to minimize sidelobe effects on the adjacent channels.

One possible spectrum solution is to separate the ISM band into four sub-bands, which are 904 - 908 MHz (Band A), 908 - 912 MHz (Band B), 918 - 922 MHz (Band C), and 922 - 926 MHz (Band D).

1.2 Sources of interference in the mobile channel

The ISM band CDMA systems present a challenge for interference mitigation. First, they must deal with traditional sources of interference such as noise and multipath. The background noise can be characterized as Gaussian. Multipath interference stems from the fact that a transmitted signal diffuses as it travels from transmitter to receiver. As a

result, a portion of the transmitted signal's power arrives directly at the receiver while other portions of the transmitted signal's power arrive after being reflected from objects such as buildings, the ground, trees, leaves, people, etc. Thus, the transmitted signal takes multiple paths to the receiver, and each path arrives delayed from the others and with a different power. This phenomenon is called multipath propagation, and it is common to all mobile channels. Multipath propagation causes the composite received signal's power to vary depending on the characteristics of the environment through which the signal travels.

Second, CDMA systems suffer from interference attributed to other CDMA users of the same band. This multiple access interference severely limits the capacity and spectral efficiency of CDMA systems. If interference rejection primarily depends on the processing gain of the spread spectrum modulation, user capacity will increase with the bandwidth. Unfortunately, larger bandwidth is not always possible in reality; however, greater channel capacity can be achieved by using interference rejection techniques.

Third, there are numerous FCC part 15 devices that use the ISM band. Because of these narrowband users, AVM systems must be able to combat interference from dissimilar modulation formats.

Fourth, some AVM service providers claim that sharing the ISM band among AVM systems could create very strong adjacent channel interference. When a mobile unit operates from the edge of the coverage region and at the same time another mobile unit

from the adjacent channel is operating close to the base station antenna, the base station will detect the close signal with a much higher power than the distant signal. RF propagation loss models indicate that the signal strength of the adjacent channel systems could be as high as 40-60 dB above that of the desired signal.

1.3 Current interference rejection techniques for direct sequence CDMA systems

There are two categories of CDMA interference rejection techniques as surveyed by Laster and Reed [Las94]. The first of these categories encompasses cyclostationary exploiting algorithms that, in many instances, resemble a fractionally-spaced equalizer (FSE). The second class of techniques use a multi-stage correlation receiver to estimate and subtract the multi-access interference.

Monogiousdis, Tafazolli, and Evans [Mon93] employ a technique based on adaptive linear fractional spaced equalization (LFSE) to adaptively cancel the multiple-access interference in CDMA systems. The simulation results indicate that the LFSE offers significant gains over the conventional detector, eliminating the near-far problem without the explicit knowledge of the interfering spreading sequences.

In a fully asynchronous single user receiver in a CDMA system, an adaptive, fractionally-spaced LMS filter, instead of matched filters with constant coefficients, can be employed for each user separately [Rap93]. The receiver is trained by a known training

sequence prior to data transmission, and continuously adjusted by an adaptive algorithm during data transmission. Experimental results show that a considerable improvement BER is achieved with respect to the conventional single-user receiver. Abjurahuman, Falconer, and Sheikh [Abj92] present related work on fractionally-spaced DF minimum mean squared error (MMSE) filters in the context of direct sequence (DS) SS CDMA. They show its performance in slow fading and how an FSE can be used as a CDMA demodulator even when slow fading is present. The advantage of this receiver is its simplicity.

For direct sequence spread spectrum (DS SS) CDMA systems, the MMSE criterion is amenable to adaptation and simple to implement, while having great near-far resistance [Mad93]. The channel output is first passed through a filter matched to the chip waveform and then sampled at the chip rate. Because of the complexity and coefficient noise associated with such an adaptive when N is large, simpler structures with fewer adaptive components are proposed. In each case the multiple samples per symbol are combined via a tapped delay line, where the taps are selected to minimize the mean square error.

Holley and Reed [Hol93] and also Aue and Reed [Aue94] show how spectral correlation properties can be exploited by a time-dependent adaptive filter (TDAF) to provide spectral capacity for CDMA using frequency-domain and time-domain filtering structures. The research suggests that by using TDAF processing, CDMA systems can

approach the same spectral efficiency as FDM/TDM systems while maintaining the advantages of wide-band modulation and universal frequency reuse.

Asynchronous CDMA systems using digital matched filtering (DMF) reception techniques suffer from poor multiple access spectral efficiency. this is due entirely to the lower bounds on the mean square cross-correlation levels which exist between the orthogonal codes allocated to each system subscriber. This interference can be estimated through channel measurement, and it is then possible to regenerate and subsequently cancel cross-correlation components from individual interfering channels.

Multi-stage correlation receivers, due to Varansi and Aazheng [Var90], are a promising suboptimal approach for reducing interference and increasing channel capacity. At each stage, a bank of single-user receivers demodulates the received signal. After each stage, the estimated signals for all interference sources are subtracted from the received signal, and then demodulation is repeated. This procedure can be repeated for an arbitrary number of stages to obtain an iterative estimate of the interference. Simulation results for a simple channel model indicate that only a few stages are necessary to achieve most of the potential performance improvement.

Most work on multistage interference rejection techniques has focused on idealized Gaussian channels and assumes perfect knowledge of each user's power. Fortunately, the use of a RAKE receiver (or similar adaptive channel estimator) in a multi-stage algorithm makes this possible. The RAKE can be used to simultaneously estimated the received data

and the channel impulse response for each user. The estimated signal will then be reconstructed and subtracted from the received signal. The new received signal is used to perform another stage of estimation. This approach allows the multi-stage receiver to form iterative estimates of both the channel and the received data, and allows the multi-stage receiver to operate with no prior information about channel condition.

Qualcomm has chosen to utilize a RAKE receiver structure. The RAKE receiver actually utilizes multipath interference to form an improved estimate of the spread spectrum signal that was transmitted. The RAKE receiver in the Qualcomm system identifies up to three delayed signal components in the channel, time-aligns the primary signal and the delayed portions of the signal, and combines the three components to achieve an improved signal-to-noise ratio (SNR) and signal-to-interference ratio (SIR). Thus, the inherent time diversity of the mobile channel is used to mitigate channel interference. Unfortunately, the performance of the RAKE receiver is limited by the time resolution of the chip interval. For Qualcomm's system, this limitation means that the RAKE receiver cannot improve performance for channels in highly urban and in-building environments in which delay path is very short.

1.4 Thesis overview

Time Dependent Adaptive Filter (TDAF) processing represents an effective approach for CDMA interference rejection. This technique is especially appropriate at the mobile

receiver where there is little prior knowledge of the spreading codes of the other users. This thesis presents enhanced forms of the Time Dependent Adaptive Filter (TDAF), which is an optimal periodically time-varying adaptive filter. It is able to fully exploit the cyclostationarity and spectral correlation in certain DS-SS signals.

In addition, it is shown how multiple AVM service providers can exist in adjacent channels within the ISM band. It is demonstrated that, using realistic channel models, the TDAF can provide substantial improvement in interference rejection over the conventional correlation receiver. Since the technique is adaptive, it is well suited for the dynamic mobile radio channel. Computationally efficient TDAF structures have been also proposed to handle the case of different code repeat intervals for different systems.

Results of CDMA overlay system simulation presented in Chapter 5 have shown that TDAF processing can achieve tremendous gain in narrowband interference rejection compared to notch/matched filter processing. The use of TDAF processing and a spectral shaping filter can also minimize the impact of adjacent channel interference. System performance shows little degradation by adjacent channel and narrowband interference.

Chapter 2

Time Dependent Adaptive Filter (TDAF) for Interference Rejection

2.0 Introduction

Recent research ([Hol93] and [Aue94]) has shown that the Time Dependent Adaptive Filter (TDAF) is superior to the conventional matched filter processing when applied to CDMA systems. For example, time dependent filtering is able to mitigate many different forms of interference common to the mobile channel. Furthermore, time-dependent filtering requires no knowledge of the other users in the system in order to produce marked increases in user capacity.

2.1 Theoretical background of time dependent adaptive filtering

In order to realize the benefit from time dependent filtering, either the desired signal or the interfering signals must exhibit the property of cyclostationarity. Cyclostationarity is a term which is used to describe the repetitive or cyclic nature of the statistics associated with a communication signal.

A process $x(t)$ is said to be cyclostationary in the wide sense if its mean and autocorrelation $R_x(t,u)$ are periodic with some period, say T_0 [Gar85]. The time-dependent autocorrelation of $x(t)$ is

$$R_{xx}(t,\tau)=E\left\langle x(t+\frac{\tau}{2})x^*(t-\frac{\tau}{2})\right\rangle$$

and

$$R_{xx}(t,\tau)=R_{xx}(t+T_0,\tau). \tag{2.1.1}$$

The variable t represents time, τ represents the lag, $E\langle\bullet\rangle$ denotes the expectation operator, T_0 represents the period of the cyclostationarity and $1/T_0$ is the cycle frequency. For most digital modulation schemes, T_0 represents the period of a baud or half the period of the carrier. Often, it is useful to define the set of cycle harmonics which are integrally related to the fundamental periodicity, T_0, as $\alpha=\frac{n}{T_0}$, where n is an integer number. Using this notation, the coefficients for the harmonic components of the cyclic autocorrelation function are given by

$$R_{xx}^{\alpha}(\tau)=\frac{1}{T_0}\int_{-T_0/2}^{T_0/2}R_{xx}(t,\tau)e^{-j2\pi\alpha t}dt\ . \tag{2.1.2}$$

Furthermore, if the range of n represents the complete set of harmonics which are integrally related to the fundamental periodicity, then the total autocorrelation may be expressed in terms of it's Fourier series expansion.

$$R_{xx}(t,\tau)=\sum_{-\infty}^{\infty}R_{xx}^{\alpha}(\tau)e^{j2\pi\alpha t}\ . \tag{2.1.3}$$

The Fourier transform of the cyclic autocorrelation is called the cyclic spectrum, $S_{xx}^{\alpha}(f)$ and is defined as

$$S_{xx}^{\alpha}(f)=\int_{-\infty}^{\infty}R_{xx}^{\alpha}(\tau)e^{-j2\pi f\tau}d\tau\ . \tag{2.1.4}$$

Similarly, the time dependent spectral density is given in as

$$S_{xx}(t,f)=\int_{-\infty}^{\infty}R_{xx}(t,\tau)e^{-j2\pi ft}d\tau\ . \tag{2.1.5}$$

These quantities provide a measure of spectral correlation between frequency components in a signal. In particular, the cyclic spectral density, $S_{xx}^{\alpha}(f)$, provides a measure of the correlation between frequency components at $f-\alpha/2$ and $f+\alpha/2$. This can be seen by taking the Fourier transform of a finite window of data,

$$X_W(t,f)=\int_{t-\frac{W}{2}}^{t+\frac{W}{2}}x(u)e^{-j2\pi fu}du\ . \tag{2.1.6}$$

and using the linearity property of the Fourier transform to rewrite $S_{xx}^{\alpha}(f)$ as

$$S_{xx}^{\alpha}(f)=\lim_{W\to\infty}\lim_{T\to\infty}\frac{1}{T}\int_{-T/2}^{T/2}\frac{1}{W}E\left\langle X_W(t,f+\frac{\alpha}{2})X_W^{*}(t,f-\frac{\alpha}{2})\right\rangle dt. \tag{2.1.7}$$

In this form, it is clear that the cyclic spectral density provides a clear measure of both the location and degree of spectral correlation in a cyclostationary process.

2.2 Spectral correlation in direct-sequence spread spectrum modulation

For a direct sequence spread spectrum system (DS-SS), the input data signal $d(t)$ is spread in bandwidth by multiplying it with a high rate spreading sequence $c(t)$. This can be viewed as the multiplication of a low-rate cyclostationary process by a high-rate cyclostationary process. Chen [Che88] has shown that there exist three fundamental periodicities in direct sequence spread spectrum signals:

- the fundamental chip rate periodicity, T_{chip} ,
- the fundamental data rate periodicity, T_{data} ,
- the fundamental code repetition rate periodicity, T_{code} .

A high degree of spectral correlation can be achieved in a DS-SS signal by carefully choosing the relationships between the three fundamental periodicities. Traditionally, the period of a data baud is chosen as an integer multiple of the chip period.

When both the data and code repetition rates are designed to be integrally related to the chip rate, then the number of fundamental periodicities in the DS-SS signal is reduced to one. Specifically, if S is defined as the number of chips per baud and N is defined as the

number of chips per code sequence repetition, then the fundamental cycle frequencies become functions of a single fundamental periodicity, T_{chip}.

$$\alpha_{chip} = \frac{1}{T_{chip}}, \tag{2.2.1}$$

$$\alpha_{data} = \frac{1}{T_{data}} = \frac{1}{ST_{chip}}, \tag{2.2.2}$$

$$\alpha_{code} = \frac{1}{T_{code}} = \frac{1}{NT_{chip}}. \tag{2.2.3}$$

The parameter S is known as the spreading or processing gain of the DS-SS signal. In order to best exploit spectral correlation of DS-SS, the data rate and code repetition rate should be integrally related, - i.e., either the ratio $\frac{S}{N}$ or the ratio $\frac{N}{S}$ must be an integer. Given this relationship, only harmonics of one fundamental periodicity α_{code} are needed by the TDAF.

2.3 Time dependent adaptive filter (TDAF) for interference rejection

The basic approach of these structures is to convert a single cyclostationary process into a collection of spectrally correlated processes. Optimal filtering is then accomplished through the optimal combination of the spectrally correlated processes to estimate every process [Ree87].

The idea behind the (TDAF) is to minimize the time-averaged difference between a desired frequency component and a linear combination of correlated frequency

components. By filtering correlated frequency components of the corrupted input signal and combining these components appropriately, a better estimate of the uncorrupted signal can be obtained.

The mathematical justification follows, given a finite window Fourier transform of the received data

$$X_T(t,f)=\int_{t-\frac{T}{2}}^{t+\frac{T}{2}} x(\tau)e^{-j2\pi f\tau}d\tau\ , \tag{2.3.1}$$

where T is the window length. This data can be filtered by a time-varying filter to produce an estimate of spectrum

$$Y_t'(t,f)=\sum_{n=0}^{N-1} W_n(f)X_T(t,f-\alpha_n). \tag{2.3.2}$$

Assuming that an uncorrupted version of the transmitted signal, $Y_T(t,f)$, is available (i.e., - a training or desired signal), the error after filtering can be computed as

$$\varepsilon_T(t,f)=Y_t(t,f)-\sum_{n=0}^{N-1} W_n(f)X_T(t,f-\alpha_n). \tag{2.3.3}$$

The objective is to determine the filters $W_n(f)$ which minimize the mean square error (MSE):

$$\text{minimize}\quad MSE=\lim_{T\to\infty}\frac{1}{T}\int_{-T/2}^{T/2}[\varepsilon_T(t,f)]^2dt. \tag{2.3.4}$$

In this equation, α_n represents the range of fundamental cycle frequencies available to the filter. The optimal filter design equation is obtained by setting the derivative of MSE with respect to $W_n(f)$ equal to zero.

$$0 = \lim_{T\to\infty} \frac{1}{T} \int_{-T/2}^{T/2} [\varepsilon_T(t,f)] X_T^*(t, f-\beta) dt, \tag{2.3.5}$$

where β is the cycle frequency for the data signal. When T is allowed to become large, the solution becomes

$$\sum_{n=0}^{N-1} W_n(f) \hat{S}_{xx}^{\beta-\alpha_n}(f - \frac{\alpha_n+\beta}{2}) = \hat{S}_{yx}^{\beta}(f - \frac{\beta}{2}) \tag{2.3.6}$$

where $\hat{S}_{xx}^{\beta-\alpha_n}(f)$ and $\hat{S}_{yx}^{\beta}(f-\frac{\beta}{2})$ represent finite time approximations of their respective cyclic spectral densities. The design of the TDAF consists of a bank of filters $W_n(f)$, each of which filters a frequency-shifted version of the input signal. The output of the TDAF is a sum of frequency-shifted and filtered signals.

An ideal frequency response may require a large number of frequency shifters and filters. Numerous phase lock oscillators and FIR filters could be very inefficient to implement. In order to minimize the overall computational count, the Discrete Fourier Transform (DFT) can be used in place of the phase locked complex oscillators to achieve the necessary frequency translation and filtering of the spectrally correlated components. If the sampling rate is chosen to be a multiple of the chip rate, then an appropriate DFT size can be chosen to exploit the spectral correlation. Figure 2.3.1 illustrates this

frequency domain structure for the optimal time dependent filter of a DS-SS signals. In this figure, it shows the estimation of i th output bin, $Y_k'(f_i)$, in the N-point FFT based TDAF structure. More details about the structure and adaptation algorithm will be described in Section 2.4.

2.4 RLS adaptation of the TDAF

The least Mean Squares (LMS) adaptation algorithm usually requires minimal computation and hardware, however it is often slow to converge, especially when the number of weights is large. Normalized and Accelerated LMS algorithms attempt to decrease the LMS convergence time by adapting the step size. However, the improved convergence rate is still too slow to track a dynamic mobile channel for the TDAF implementation.

Compared to the LMS algorithm, the Recursive Least Squares (RLS) algorithm is very attractive due to its fast convergence, relative insensitivity to the Eigenvalue spread, and lower steady-state mean square error [Hol93]. The major drawbacks of the RLS algorithm are it's increased computation count and storage requirements. The RLS algorithm can be utilized for time-dependent filtering to adaptively combine spectrally correlated portions of the signal spectrum in the following manner.

The RLS adaptation algorithm attempts to minimize the least squares error between a desired frequency component and a linear combination of correlated frequency

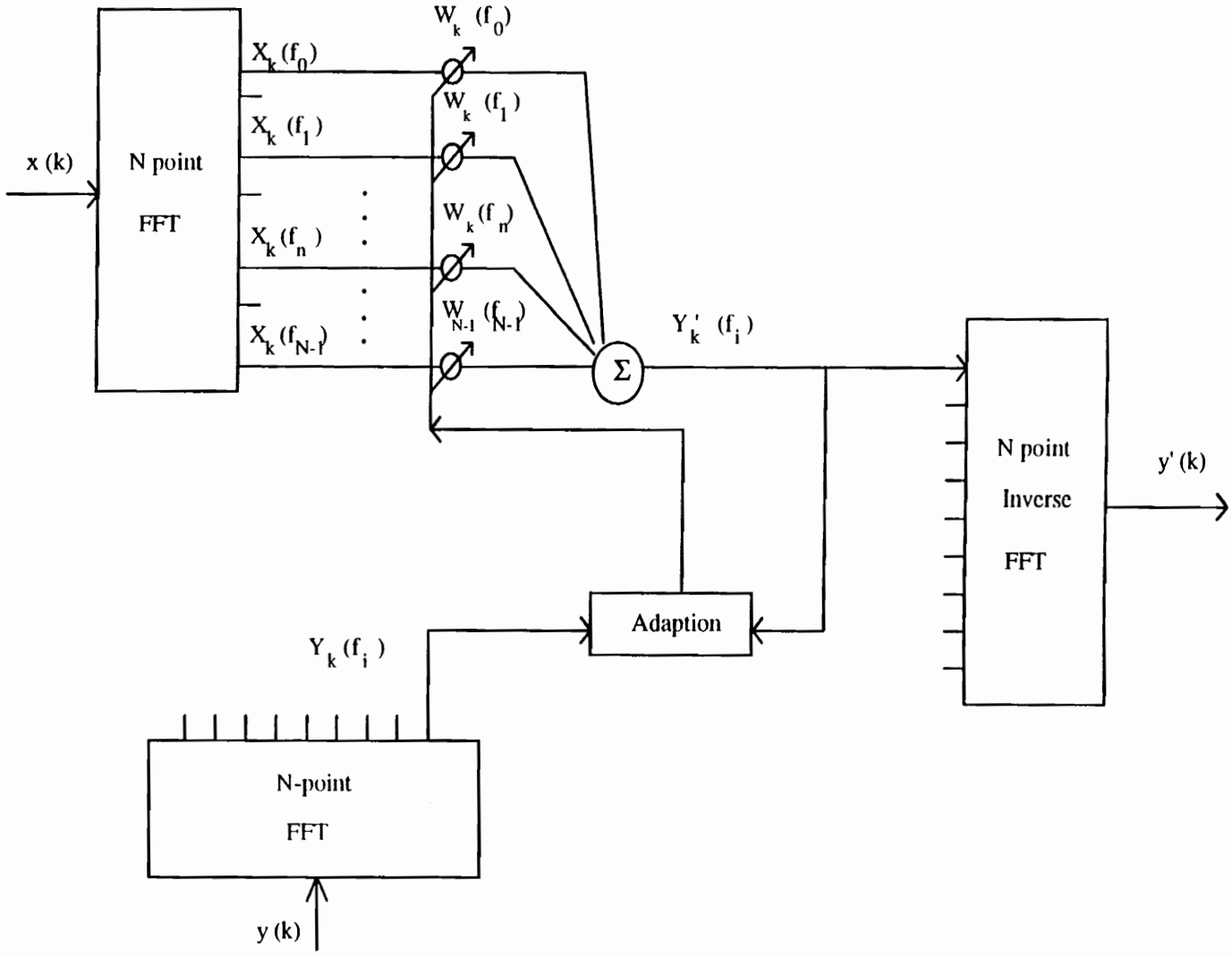

Figure 2.3.1 FFT based optimal Time dependent adaptive filter structure showing the estimation of one output bin

components. It is assumed that the sample rate of the input signal is an integer multiple of the fundamental code repeat rate. The transformed input vector is then given by

$$X_k(f_i) = i\text{'}th\ bin\ FFT\ [x(k)\ x(k-1)\ \cdots\ x(k-N+1)]^T\ . \tag{2.4.1}$$

The corresponding weight vectors will be a row of a single $N \times N$ matrix

$$W_k^0 = \begin{vmatrix} W_{0,0}^0 & W_{0,1}^0 & \cdots & W_{0,N-1}^0 \\ W_{1,0}^0 & W_{1,1}^0 & \cdots & W_{1,N-1}^0 \\ \cdot & & & \cdot \\ & & & \\ \cdot & & & \cdot \\ W_{N-1,0}^0 & W_{N-1,1}^0 & \cdots & W_{N-1,N-1}^0 \end{vmatrix}. \tag{2.4.2}$$

The inverse spectral correlation matrix R_{k-1}^{-1} of the TDAF are initialized as

$$R_{k-1}^{-1} = \eta \cdot I\ , \tag{2.4.3}$$

where η is chosen as a large positive constant and I represents the $N \times N$ identity matrix. The elements of the a priori frequency-domain output bins are computed in scalar form as

$$\hat{Y}_k^{\alpha}(f_i) = \sum_{n=-l}^{u} W_{k-1,n}^0(f_i) \cdot X_{k,n}(f_i + \alpha_n)\ . \tag{2.4.4}$$

The range of n is defined to be $n \in \{-l, u\}$ so that $X_k(f_i + \alpha_{-l})$ and $X_k(f_i + \alpha_u)$ lie within the possible FFT bins. In matrix form, it can represented as the product of the weight matrix and the input FFT bins

$$\hat{Y}_k^{\alpha} = W_{k-1}^{0} X_k \ . \tag{2.4.5}$$

In this form, each bin of $\hat{Y}_k^{\alpha}$ is formed from a linear combination of all the input bins. After forming the priori output estimate, the frequency-domain error vector is computed as

$$E_k = Y_k - \hat{Y}_k^{\alpha}, \tag{2.4.6}$$

or in scalar form as

$$E_k(f_i) = Y_k(f_i) - \hat{Y}_k^{\alpha}(f_i). \tag{2.4.7}$$

The frequency-domain gain vector is then computed based on the vector product of the inverse spectral correlation matrix and the current frequency-domain input vector. The complete RLS adaptation algorithm for TDAF is presented in Table 2.4.1.

2.5 Blind equalizer algorithm for the TDAF

The blind adaptation of time dependent filter [Hol93], i.e. the actual signal is not available, is very similar to the adaptation algorithm for training sequence. After convergence of the TDAF, the output approximates the desired signal and can be used to train the filter. A decision Feedback Equalizer (DFE) adaptation is obtained by making a

Table 2.4.1 RLS adaptation algorithm for the TDAF

$$W_{k-1}^{0} = 0 \cdot I$$

$$R_{k-1}^{-1} = \eta \cdot I$$

$$X_k(f_i) = i\text{'th bin of } FFT\,[x(k)\ x(k-1) \cdots x(k-N+1)]^T$$

$$\hat{Y}_k = W_{k-1}^{0} X_k$$

$$E_k = Y_k - \hat{Y}_k$$

$$Z_k = X_k^H R_{k-1}^{-1}$$

$$Q = Z_k X_k$$

$$V = \frac{1}{\rho + Q}$$

$$\tilde{Z}_k = V \cdot R_{k-1}^{-1} X_k$$

$$R_k^{-1} = \frac{1}{\rho}[R_{k-1}^{-1} - \tilde{Z}_k Z_k]$$

$$W_k^{0} = W_{k-1}^{0} + E_k \tilde{Z}_k^H$$

$$[\tilde{y}^{\alpha}(k)\ \tilde{y}^{\alpha}(k-1) \cdots \tilde{y}^{\alpha}(k-N+1)]^T = FFT^{-1}[\hat{Y}_k]$$

$$[\tilde{y}^{p}(k)\ \tilde{y}^{p}(k-1) \cdots \tilde{y}^{p}(k-N+1)]^T = FFT^{-1}[W_k^{0} X_k]$$

maximum likelihood estimate of the transmitted symbol based on the filter output, $\hat{y}(k)$, and using this "best guess" as the training or desired sequence, $y(k)$. For a binary system, the valid symbol would be either +1 or -1. Having selected the best symbol estimate, the error is determined by

$$\begin{aligned} e(k) &= s_c - \hat{y}(k) \\ &= y(k) - \hat{y}(k) \end{aligned} \quad . \tag{2.5.1}$$

Although the Recursive Least Square (RLS) based DFE represents one of the fastest converging and best tracking combinations for the mobile channel, it can fail to converge when the decision error rate grows sufficiently high.

For BPSK, the ideal constellation diagram for the demodulated data is represented by $s_c(i)$ of +1 or -1. If the real part of demodulated data, $d(i)$ is positive, it corresponds to demodulation data of +1; otherwise, it corresponds demodulation data of -1. Although the distance between $d(i)$ and $s_c(i)$ varies from one data to data, the traditional RLS-DFE will weight the decisions for any $d(i)$ equally. In order to incorporate the strength of the decision into the RLS-DFE algorithm, weight update equation can be modified as

$$W_k^0 = W_{k-1}^0 + \psi_k \cdot E_k \tilde{Z}_H \tag{2.5.2}$$

where ψ_k becomes a scalar quantity by which the least squares update is scaled, $\tilde{Z}_H$ is the gain vector. The traditional form of the RLS based DFE is realized by setting $\psi_k = 1$. However, by defining ψ_k as a function of the frequency domain error vector, an improved adaptation can be obtained.

In the time domain, the most simple measure for ψ_k is the value of the normalized power in the error. Since the time domain error out of the demodulator is given by (2.5.1), the power of the error output can easily be computed as

$$Err = e(k)e^{*}(k). \tag{2.5.3}$$

For BPSK modulation, the minimum distance between constellation points is $d_{\min} = 2$. It is desirable to compute the scale factor from the frequency domain error vector E_k. The most common adaptation in neural networks is the exponential or Gaussian function. It is desirable to compute the scale factor from the frequency domain error vector ψ_k can be defined as

$$\psi_k = e^{-\left[\frac{I}{R_b^2}\right]}, \quad 0 < \psi_k \leq 1 \tag{2.5.4}$$

where R_b^2 is the normalization radius given by

$$R_b^2 = \frac{d_{\min}^2}{4\sqrt{-\ln p}}. \tag{2.5.5}$$

where $d_{\min}$ is the distance between ideal spot $s_c(i)$ to demodulated value $d(i)$ in the constellation diagram. The constant p represents the degree of influence which a boundary value point from the filter should have no the weight update equation. For instance, $p = 0.01$ implies that a filter output which is located at an error radius of $d_{\min}/2$ should have only 1% of the influence of a filter output located directly on a valid constellation point. This new algorithm, as shown in Table 2.5.2 is designated as the Exponential Law DFE or EDFE [Hol93].

Table 2.5.2 Exponential-law DFE algorithm for the TDAF

$$W_{k-1}^{0} = 0 \cdot I$$

$$R_{k-1}^{-1} = \eta \cdot I$$

$$X_k(f_i) = i' \text{ th bin of } FFT\ [\ x(k)\ x(k-1)\ \cdots\ x(k-N+1)]^T$$

$$\hat{Y}_k = W_{k-1}^{0} X_k$$

$$E_k = S_c - \hat{Y}_k$$

$$Z_k = X_k^H R_{k-1}^{-1}$$

$$Q = Z_k X_k$$

$$V = \frac{1}{\rho + Q}$$

$$\tilde{Z}_k = V \cdot R_{k-1}^{-1} X_k$$

$$R_k^{-1} = \frac{1}{\rho}[R_{k-1}^{-1} - \tilde{Z}_k Z_k]$$

$$T = \left[\frac{1}{N^2}\right] E_k^H E_k$$

$$\psi_k = e^{-\left[\frac{T}{R_D^2}\right]}$$

$$W_k^{0} = W_{k-1}^{0} + \psi_k \cdot E_k \tilde{Z}_k^H$$

$$[\hat{y}^{\alpha}(k)\ \hat{y}^{\alpha}(k-1)\ \cdots\ \hat{y}^{\alpha}(k-N+1)]^T = FFT^{-1}[\hat{Y}_k]$$

$$[\hat{y}^{p}(k)\ \hat{y}^{p}(k-1)\ \cdots\ \hat{y}^{p}(k-N+1)]^T = FFT^{-1}[W_k^{0} X_k]$$

For a very dynamic channel, the EDFE algorithm, slowly moves the weight vector towards the optimal solution. In addition, the EDFE is less sensitive to impulsive or

transient interference than the DFE. Once convergence is achieved, the EDFE behaves in manner similar to the DFE where the scale factor is approximately unity.

Chapter 3

Improved TDAF Structures

3.0 Introduction

In previous the TDAF structure, the FFT size must be the same as the *number of samples per code repetition period*; however, the FFT size needs to be a power of two to be computationally efficient. If the signal-non-of-interest (SNOI) has a different code repeat rate than the signal-of-interest (SOI), the classic TDAF structure does not perform well, because it is not periodic at a rate commensurate with the statistic at the SNOI. Thus it is necessary to modify the TDAF structure.

3.1 TDAF with adjustable input block size

The code repetition period is the fundamental cycle frequency for a code on pulse spread spectrum (SS) signal. The input signals are processed block by block in TDAF with a fundamental periodicity corresponding to the code repeat rate. That is, the TDAF input signal block size is chosen to be the same as the *number of samples per code repetition period* and the FFT size equals the input signal block size. That is, the data and the filter are time synchronized.

If the FFT size is greater than the block size of the input signal, the remaining part of the FFT block can be zero padded. The signal is still cyclostationary after zero padding; however, the input signal inside a FFT input block should contain at least one whole code repetition period. Another critical point is that the code should be at the same point in the input block for each new block.

In practice, signals are processed block by block, the block size corresponds to the *number of samples per code repetition period* of SOI. The block size must be equal to the code period for the filter periodicity to be commensurate with the statistical periodicity of the signal. Without this property, the TDAF will not operate well. When co-channel CDMA signals with different code repeat rates are added, the TDAF structure will not be

The FFT size N should be larger than the original data block size M. When the input block of M points does not match the N point FFT size, N-M zeros are appended to the input signals and at the IFFT output, the first M points are extracted. Ideally N should be a power of two or four to use the most efficient FFT algorithms. The new TDAF structure is presented in Figure 3.1.1.

3.2 Long FFT and switching long FFT structures

If several independent systems share the same frequency band, it is possible to have a mixture of CDMA signals with different signal parameters. In particular, the different

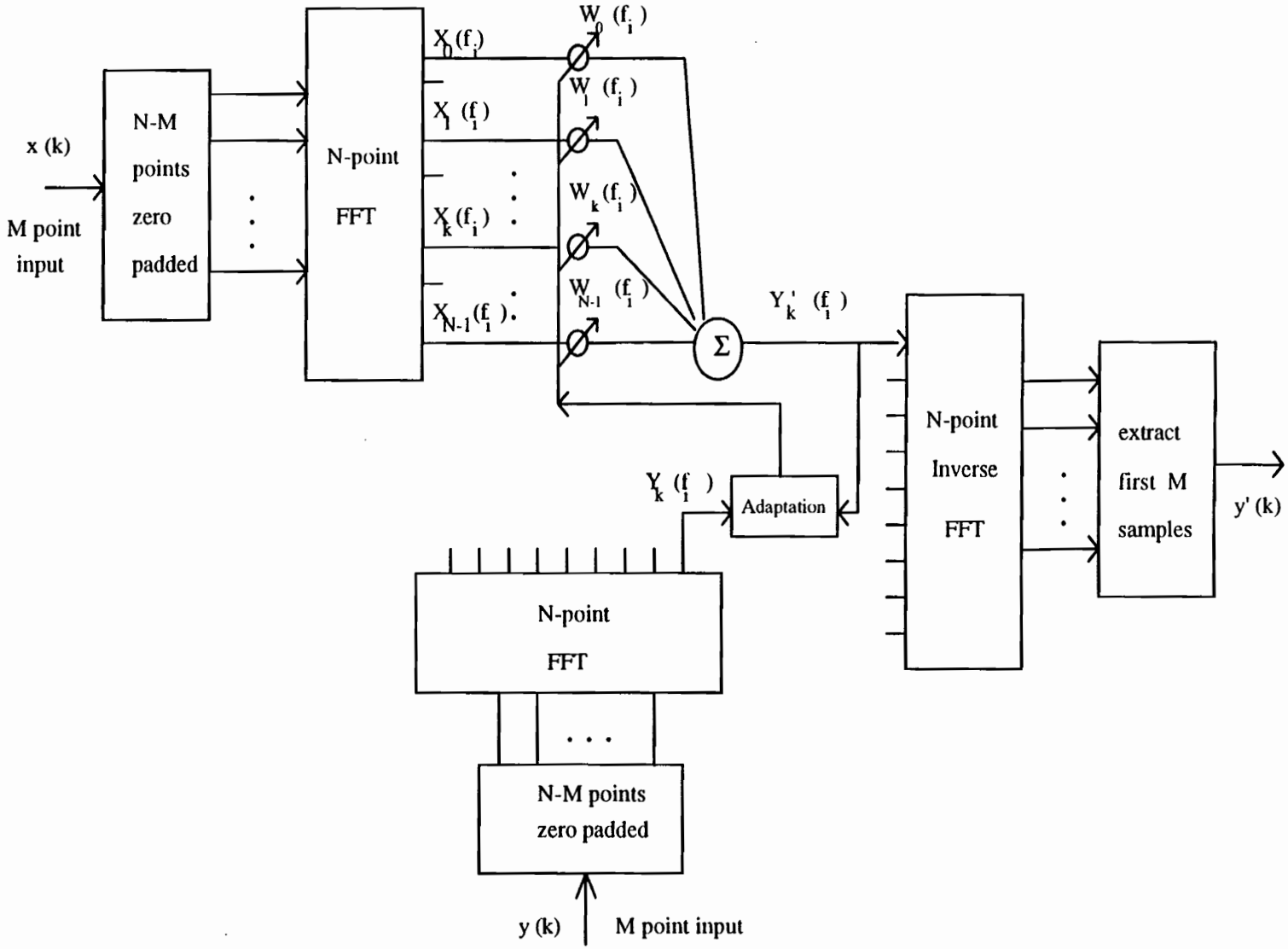

Figure 3.1.1 Time Dependent Adaptive Filter with an adjustable input block size

systems could have different code repetition rates. Therefore co-channel interference can come from users of the same system, as well as users from other CDMA system users.

In practice, signals are processed block by block, the block size corresponds to the number of samples per code repetition period of SOI. The block size must be equal to the code period for the filter periodicity to be commensurate with the statistical peridocitiy of the signal. Without this property, the TDAF will not operate well. When co-channel CDMA signals with different code repeat rates are added, the TDAF structure will not be periodic with their code repeat rates. The filter is only periodic at a rate commensurate with the statistical periodicity for one particular code repeat rate. This means that a particular point in the code interval will at the same position in the input block, thus effectively transforming the cyclostationary signal into a vector stationary signal.

For example, if the *number of samples per code repetition period* for any user is less than the selected block size, the signal would be truncated. The remaining samples will attach to the next input block with the signals from next code repetition period. In this case, the filter is not periodic at a rate commensurating with the underlying statistical periodicity (the code repeat rate). Since the code does not appear at the same spot at every input block, the signal can not be converted to a vector stationary process.

If the *number of samples per code repetition period* for any user is larger than the selected block size, input block will be filled with a portion of signal in the next code repetition period; therefore the code does not appear at the same place for every input block, the signal is not converted to a vector stationary process.

Because the SOI is additive with the SNOI, using zero padding to compensate for an imperfect FFT size is not a solution. The TDAF performance for this type CDMA interference is poor. One solution is to use a TDAF with a long FFT size. The fundamental issue for successful TDAF processing is that the code remains at the same relative position within every input block. If a block size is an integer times of *number of samples per code repetition period*, each block will also have the same property. It is possible to find a number which will contain an integer for all *number of samples per code repetition periods* from different systems.

The long block will cover an integer number of code repetition periods for the SOI and SNOI. This integer number can be different for the SOI and SNOI. In this way, the timing of the code within the block remains constant from block to block. The block diagram for the long FFT structure is essentially the same as for the traditional TDAF structure in Figure 2.1.1, except for a much longer FFT size. If necessary the input signal can be zero padded to use an efficient FFT size.

This new input block size can be viewed as increasing the original code repeat period by an integer. Thus, all the users have the same long code repeat period. To reduce the complexity in the CDMA system, a code length equal to some power of two will be used. This means that it is easy to find a common integer multiple, as well as extended code period.

Using a long FFT based TDAF structure makes it is possible to do interference rejection in an environment which has different code repeat rates. However, there are some disadvantages to this long FFT approach. First, it requires much more memory, the size of weight matrix in TDAF is decided by the FFT size, and the number of weights increases with the square of FFT size, and so does the computation. Second, a new longer code repetition period slows the convergence rate. Finally, the latency time (delay introduced by the processing) is also increased.

By increasing the block size N by a factor of P, the fundamental periodicity is now $1/PN$. As the TDAF is periodic at multiple of this harmonic $1/N$, it is also periodic at the code repeat rate. Although, the SOI and SNOI use different code repeat rates, they repeat a different number of times within the long input block, but the pattern in a long block is repeated in the next block.

In a switching FFT structure as Figure 3.2.1, input signals are separated to several sub-blocks, and each weight matrix corresponds to a particular sub block inside the large block. The switch in TDAF circles between these weight matrices periodically. The FFT bins are periodically filtered by these switching filters.

The switching FFT structure breaks a long block length into P sub-blocks.

$$N \cdot P = L \tag{3.2.1}$$

where N is *number of samples per code repetition periods* of SOI, L is the size of one

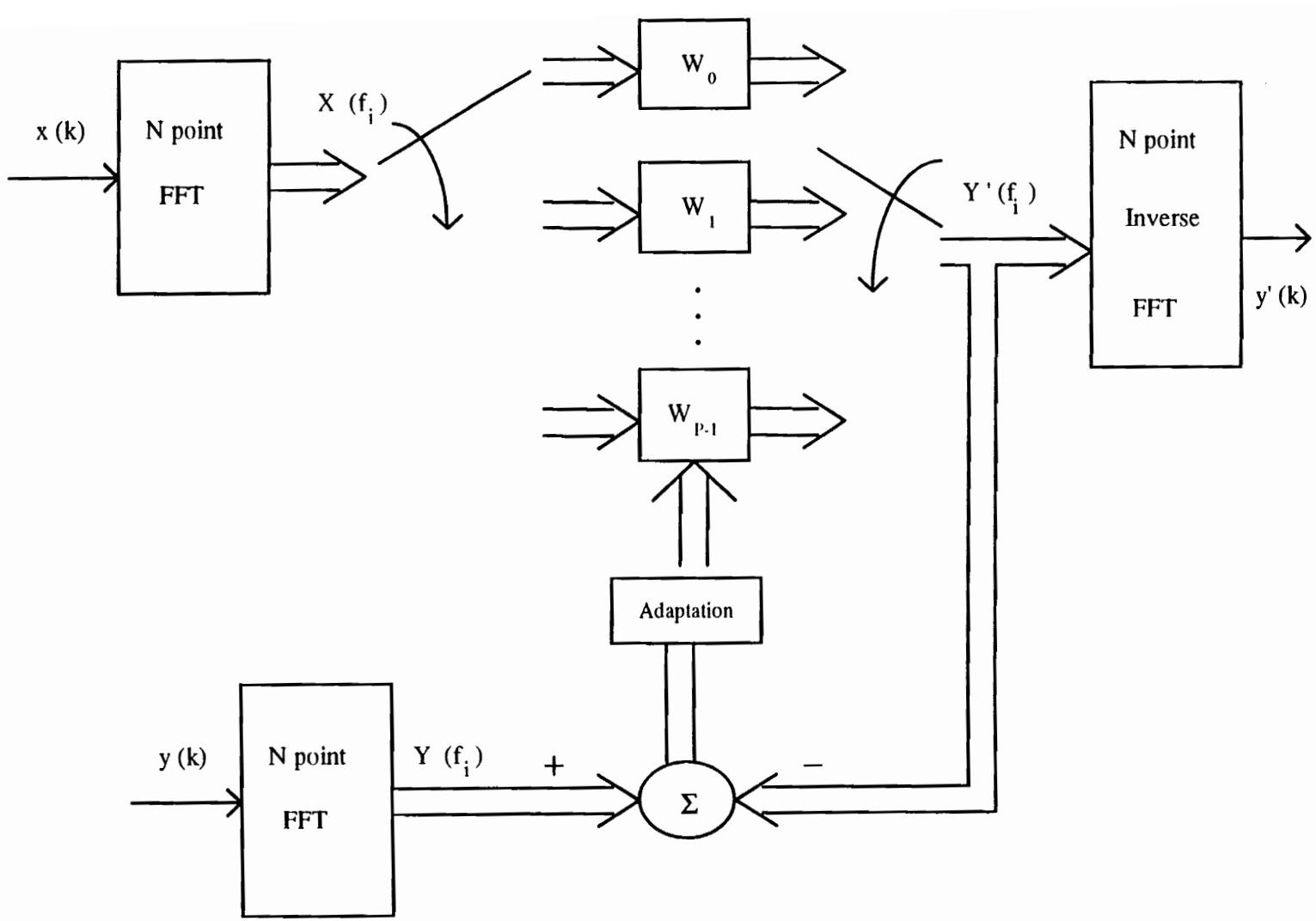

Figure 3.2.1 Switching FFT TDAF structure

long input block. Here in a switching FFT structure, the FFT size is chosen to be N. The adaptation algorithm for TDAF is shown Table 3.2.1.

Table 3.2.1 Exponential-law DFE algorithm for switching FFT structure TDAF

$$W_{k-1}^{p} = 0 \cdot I$$

$$R_{p,k-1}^{-1} = \eta \cdot I$$

$$X_k(f_i) = i^{th}\ bin\ of\ FFT\ [\ x(k)\ x(k-1)\ \cdots\ x(k-N/P+1)]^T$$

$$\hat{Y}_k = W_{k-1}^{p} X_k$$

$$E_k = S_c - \hat{Y}_k$$

$$Z_k = X_k^H R_{k-1}^{-1}$$

$$Q = Z_k X_k$$

$$V = \frac{1}{\rho + Q}$$

$$\tilde{Z}_k = V \cdot R_{p,k-1}^{-1} X_k$$

$$R_{p,k}^{-1} = \frac{1}{\rho}[R_{p,k-1}^{-1} - \tilde{Z}_k Z_k]$$

$$T = \left[\frac{1}{N^2}\right] E_k^H E_k$$

$$\psi_k = e^{-\left[\frac{T}{R_b^2}\right]}$$

$$W_k^p = W_{k-1}^p + \psi_k \cdot E_k \tilde{Z}_k^H$$

$$[\hat{y}^{\alpha}(k)\ \hat{y}^{\alpha}(k-1)\ \cdots\ \hat{y}^{\alpha}(k-N+1)]^T = FFT^{-1}[\hat{Y}_k]$$

$$[\hat{y}^{b}(k)\ \hat{y}^{b}(k-1)\ \cdots\ \hat{y}^{b}(k-N+1)]^T = FFT^{-1}[W_k^p X_k]$$

$$p = (p+1) \bmod P$$

For a long FFT structure, the estimated computation for L output points will be $7\times L^2+L\times\log_2 L$ multiplications and $7\times L^2+L\times\log_2 L$ additions, where L is the FFT size in the long FFT based TDAF. In a switching FFT structure, the number multiplications is expected to be reduced to $7\times L^2/p+L\times\log_2(L/p)$, and the additions will be $7\times L^2/p+L\times\log_2(L/p)$. The reduce factor for estimation computation is p. It is assumed that additions and subtractions are one floating operation if real and two if complex, multiplications and divisions count one operation each if the result is real and six operations if it is not. The estimated operations and MATLAB operation counts for long FFT structure and switching FFT structure are listed in the Table 3.2.2. It is assumed that the long input block is separated in *P=4* sub-blocks.

Table 3.2.2 Computation comparison between the long FFT and switching FFT structures

	long FFT Structure		switching FFT Structure		
size L	estimated	simulated	estimated	simulated	reduction factor
64	232,310	235,770	69,736	71,840	3.281
128	923,894	927,783	234,712	247,476	3.749
256	3,683,830	3,688,372	9,429,240	943,038	3.911
512	14,709,750	14,715,201	3,695,576	3,711,132	3.965

The switching long FFT can significantly reduce the requirement of memory and computation. A large weight matrix will be replaced by several smaller weight matrices. The total number of weights in the matrices will be reduced from P^2N^2 to PN^2. The reduce factor for memory is a factor of P.

Representative parameters in the performance test case for the long FFT and switching FFT structure based TDAFs is shown in Table 3.2.3. Results in Table 3.2.4 shows that

Table 3.2.3 Performance test parameters for TDAF

co-channel users:	15
SNR:	20 dB
power variance:	0 dB
SOI processing gain:	48, or 16.8 dB
samples per chip:	2
SOI number of samples per code repetition period: 96	
SNOI number of samples per code repetition period: 128	

the memory requirement for the switching FFT structure is much lower than that of the long FFT structure. At the same time, the SIR at the output for both structures have little difference, i.e., the switching FFT based TDAF can significantly reduce the computation and memory requirement while maintaining the same level of processing quality.

Table 3.2.4 Performance and memory requirement comparison

	long FFT structure	switching FFT structure
FFT size	384	96
SIR at output	29.02 dB	28.94 dB
total weight matrices size	147456	36864

Chapter 4

Channel Model for Automatic Vehicle Monitoring Systems

4.0 Introduction

This chapter describes typical channel models for mobile communications. Models for ISM band CDMA AVM system signals and interference are also described. These signals and channel models are used in Chapter 5 to simulate the performance and capacity of AVM systems.

4.1 Co-channel interference

When a frequency band is shared by using spread-spectrum modulation, each user is assigned a different spreading code so that they can be separated by the receiver despreading process. The despreading operation is performed by correlating the received signal with the spreading code of the desired user. Interference from a user with a different spreading code is determined by the cross-correlation between the spreading codes of the SOI and interference.

In a cellular systems, the full-duplex radio channel is provided using one frequency band for transmission from the cell-site to the mobile unit and a different frequency band for transmission from the mobile unit to the cell-site. The frequency separation allows a mobile unit's transmitter and receiver to be active simultaneously.

Co-channel interference level depends on path loss. A significant loss of capacity results when co-users of the spectrum have different power levels, and thus the system needs power control. Power control is not feasible when non-cooperative systems operate in the same band and thus there may be a significant loss of capacity.

In the simulations which follows in Chapter 5, perfect power control is assumed, so that for co-operative system users the received power from each mobile unit is the same. Signals transmitted from each mobile unit arrive at the base station along a different path. And, different users' signals are not time aligned. Therefore the received signal is the summation of all users' signals with random phase and time delay from for different users.

4.2 White Gaussian noise

Thermal noise due to thermal motion of electrons in resistive elements is present in all communication systems. Thermal noise can be described as an additive zero-mean Gaussian random process. In order to compare different systems without the need of specifying the noise bandwidth, energy per bit to noise spectral density, E_b/N_o is usually used as a measure of noise. In the simulations, the mean signal level is held constant while

the added noise power is changed to obtain a BER analysis as a function of E_b/N_o. Specifically, a random variable, n, representing white Gaussian noise with zero mean and variance σ^2 is added to each sample of the signal.

4.3 Spectral shaping filtering

As proposed by some AVM companies, the ISM band could be allocated into four sub-bands each with 4 MHz bandwidth dedicated to a particular system. The 4 MHz bandwidth is referred to as the first null-to-null bandwidth; therefore the mainlobe of an AVM system has to be located on the sidelobe of an adjacent system.

Strong leakage of sidelobe energy may severely reduce the capacity of the adjacent channel system. In order to minimize sidelobes before transmission, a spectral shaping filtering must be used. This can be achieved either by using a raised cosine filter at the transmitter or a square root raised cosine filter at both the transmitter and the receiver.

It is more advantageous to use the square root raised cosine filter, because by placing square root raised cosine filters in both a transmitter and receiver, both Nyquist pulse shaping and matched filtering are achieved. The transfer function of a square root raised cosine filter is defined as the square root of the transfer function of a raised cosine filter, which can be expressed as

$$H_{\sqrt{R_c}}(f)=\begin{cases}1 & 0\le|f|\le\frac{r_b}{2}(1-\alpha)\\ \cos\left\{\frac{\pi}{2\alpha r_b}\left[|f|-\frac{r_b}{2}(1-\alpha)\right]\right\} & \frac{r_b}{2}(1-\alpha)\le|f|\le\frac{r_b}{2}(1+\alpha)\\ 0 & |f|\ge\frac{r_b}{2}(1+\alpha)\end{cases}, \quad (4.3.1)$$

where r_b is the symbol rate and α is the rolloff factor. The frequency response for raised cosine filter with different rolloff factors are shown in Figure 4.3.1.

Using the inverse Fourier transform, the impulse response can be obtained as

$$h_{\sqrt{R_c}}(kT)=\frac{1}{M}\sum_{n=0}^{M-1}H_{\sqrt{R_c}}(\frac{n}{MT})e^{\frac{j2\pi nk}{M}} \quad (4.3.2)$$

$$k=0,1,\cdots,M-1\ .$$

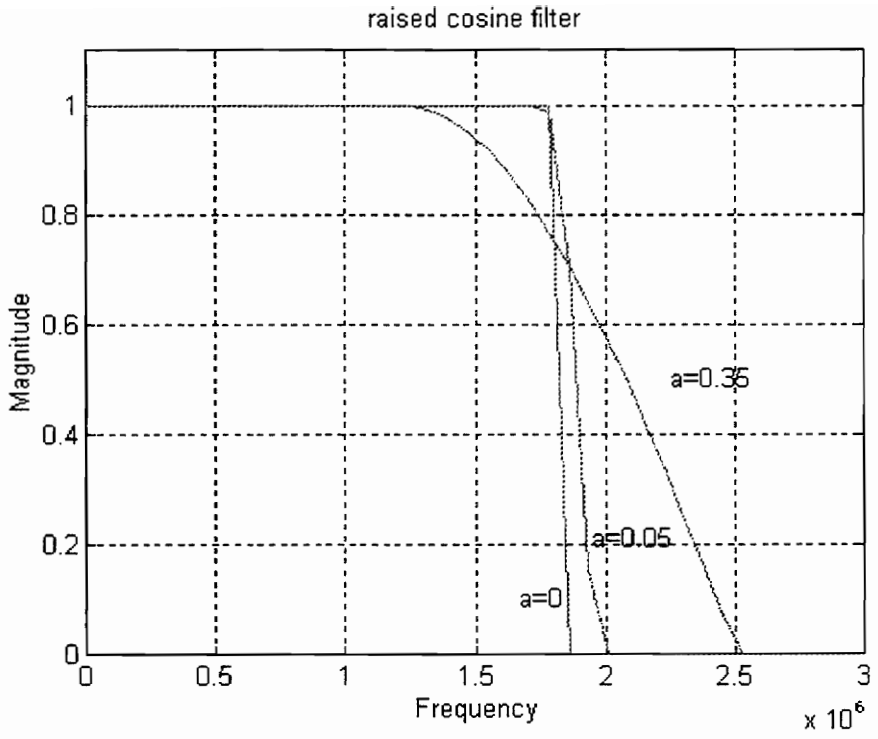

Figure 4.3.1 Frequency response of raised cosine filter with different rolloff factors

The signal at the output of the matched filter is

$$r(kT_s) = h_{\sqrt{R_c}}(kT_s) * h_{\sqrt{R_c}}(kT_s). \qquad (4.3.3)$$

$$k = 0,1,\cdots, M-1 .$$

The baud rate that a communication system can support without ISI is related to the absolute bandwidth of the systems and the rolloff factor of the raised cosine filter. Representative parameters of an AVM system are shown in Table 4.3.1 and used in the analysis of the performance of the TDAF.

Table 4.3.1 Raised cosine filter parameters

Modulation type	BPSK
available bandwidth	4 MHz
data rate	28.8 kbits/sec
processing gain	64 (or 18 dB)
chip rate	1843.2 kHz
sample rate	3686.4 kHz
raised cosine factor	0.05
FIR filter length	64

Figure 4.3.2 and Figure 4.3.3 compare the magnitude spectrum of the CDMA signal before and after the spectral shaping filtering. The DS-SS signal with 4 MHz bandwidth is represented in a complex baseband form.

In Figure 4.3.2, the maximum magnitude of the first sidelobe is only -13 dB down from peak magnitude in the mainlobe. In Figure 4.3.3 the peak of the first sidelobe of the filtered signal is attenuated to -26 dB from the peak of original mainlobe signal. The 13 dB additional attenuation achieved by the spectral shaping filtering significantly reduces the adjacent channel interference level.

Although spectral shaping filters can greatly reduce sidelobe energy, it may also introduce distortion. Generally, a higher order filter is used for minimizing the distortion; however, in this case the distortion caused by spectral shaping filtering is limited to a small

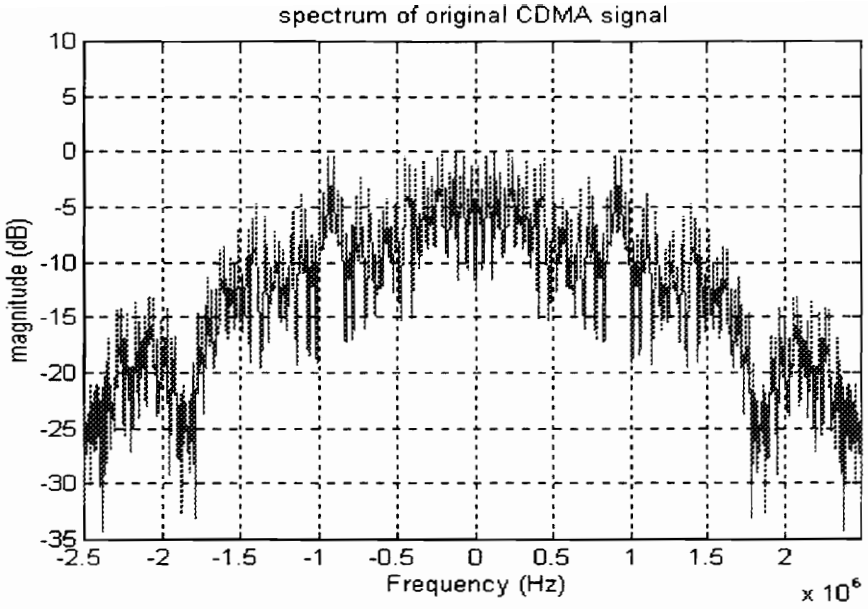

Figure 4.3.2 Spectrum of the unfiltered CDMA signal

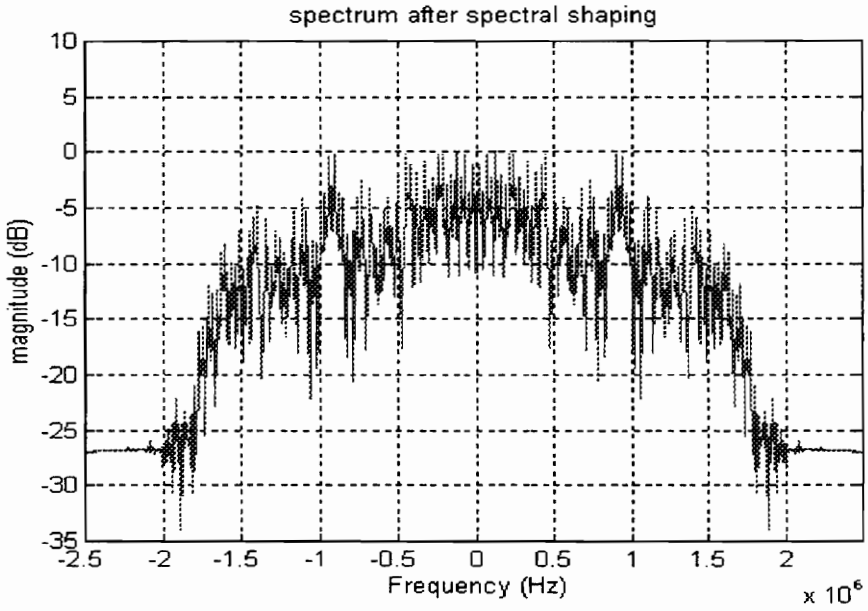

Figure 4.3.3 Spectrum after spectral shaping

portion of the spectrum that is close to edge of the band. Interference rejection techniques, such as the Time-Dependent-Adaptive-Filter (TDAF) have significant capability for interference mitigation. Simulation results show that a CDMA signal distorted by the spectral shaping filter can be improved by using TDAF processing. The system suffers very little distortion; therefore, a high order or expensive filter is not necessary.

4.4 Adjacent system interference

According to the proposals filed by potential AVM service providers, there can be up to four systems using the ISM band. Direct overly on all systems does not appear to be feasible with current technology; however, partial overlay among systems will allow one system to locate its mainlobe on the sidelobe of the adjacent system.

Although, spectral shaping filters will be used to minimize the sidelobe effect of adjacent systems, the near-far power difference could significantly raise the adjacent channel interference level.

For users in the same system, spreading codes are used to separate different users and power control can equalize the signal strength levels. In practice, codes used by adjacent systems are viewed as random codes to the users in the primary channel.

4.5 Model for geographical distribution of users

Power control and the geographical distribution of users can have an influence on the coverage and capacity of CDMA systems. Although, FCC regulations restrict transmit power for users in the ISM band, the path loss from mobile units to the base station antenna may vary greatly. If a transmitter antenna is located in free space, i.e, remote from the earth or any obstructions, then it has a gain G_T in the direction towards a receiver antenna. The power density at a distance d meters in the chosen direction is [Par93]

$$W=\frac{P_T G_T}{4\pi d^2} . \tag{4.5.1}$$

The available power at the receiving antenna, which has an effective area A is

$$P_R = \frac{P_T G_T}{4\pi d^2} \cdot A , \tag{4.5.2}$$

and A is defined as

$$A=\frac{\lambda^2 G_R}{4\pi} , \tag{4.5.3}$$

where G_R is the gain of the receiving antenna, P_T, P_R are transmitted and received power.

Thus, we obtain

$$\frac{P_R}{P_T} = G_T G_R \left[\frac{\lambda}{4\pi d}\right]^2 , \tag{4.5.4}$$

which is a fundamental relationship known as the free space or Friis equation. Using the well known relationship between wavelength λ, frequency f and velocity of propagation ($c=\lambda f$), the propagation loss (or path loss) L_F is conveniently expressed in dB as

$$L_F = 10\log_{10}\frac{P_R}{P_T} \tag{4.5.6}$$

$$=10\log_{10} G_T + 10\log_{10} G_R - 20\log_{10} f - 20\log_{10} d + k,$$

where

$$k=20\log_{10}\frac{3\times 10^8}{4\pi}=147.6\ .$$

This equation is known as a free-space propagation model [Bul77]. The free-space propagation equation applies only under very restricted conditions; in practical situations there are almost always obstructions in the propagation path from which the radio waves are reflected. A very simple case, but one of practical interest, is that of propagation between two elevated antennas within line of sight of each other.

For distance d less than a few tens of kilometers, it is often permissible to neglect earth curvature and assume that the surface is smooth and flat. The plane-earth propagation modeled is

$$\frac{P_R}{P_T} = G_T G_R \left(\frac{h_T h_R}{d^2}\right)^2\ , \tag{4.5.7}$$

where h_T and h_R represent the height of the transmitter and receiver antennas. It differs from the free-space relationship in two important ways. First as a consequence of the

assumption that $d>>h_T, h_R$, the angle between the line of two antenna and earth surface is small, the equation becomes frequency-independent. Secondly, it shows an inverse fourth-power law for attenuation instead of the inverse square law. This means a far more rapid decrease in received power.

A convenient logarithmic form for Eq. 4.5.7 can be written

$$L_P = 10\log_{10} G_T + 10\log_{10} G_R + 20\log_{10} h_T + 20\log_{10} h_R - 40\log_{10} d. \qquad (4.5.8)$$

In the simulation, the location of all the mobile units are randomly distributed. A typical cell site may have a 1-3 miles coverage radius in urban and suburban areas, and 3-8 miles in rural areas. Here it is assumed that co-system CDMA users have perfect or nearly perfect power control; however, there is no power control among all the adjacent systems or part 15 devices with respect to the intended receiver.

According to the FCC regulations, an ISM band device should operates at a fairly low power level; however, propagation path loss from mobile units to base station antennas varies significantly. Without universal power control, a non-system unit closer to the base station will detected to have a relatively higher power. To better model the effect of propagation conditions on signal strength, it is assumed that there is a breakpoint for the propagation characteristics between a mobile unit and base station. Any mobile unit which locates inside the circle of breakpoint distance is assumed to have line-of-sight coverage and path loss is predicted by the free space model. Outside this range, radiowave propagation will have little chance of line-of-sight coverage; therefore, it is modeled by the

plane earth model. As analyzed before, the plane earth model differs from the free space model in that path loss increases with fourth power law instead of the square law.

In the simulations, mobile units' locations are uniformly distributed inside the cellsite coverage area, and the shape of cellsite coverage is a circle. The probability density $p(d)$ of N number of mobile units in the coverage area is

$$p(d) = \begin{cases} \dfrac{N}{2R^2} & 0<d<R \\ 0 & otherwise, \end{cases} \tag{4.5.9}$$

where R is cellsite coverage radius, d is the distance towards the cellsite. Figure 4.5.1 shows 40 uniformly distributed users inside the cellsite coverage area. Here, the cellsite coverage radius is 8 miles, the SOI unit is operating at the edge of the cellsite coverage, (marked by '*'). Those who are located inside the inner circle are assumed to have line-of-sight coverage. The total power is the sum of uniformly distributed users' signal power.

4.6 Narrowband interference

According to FCC regulations, unlicensed part 15 devices can operate in the ISM band. Wideband users, including the proposed AVM systems, share the ISM band with the narrowband users. Both narrowband and wideband users are restricted to transmit at a low power.

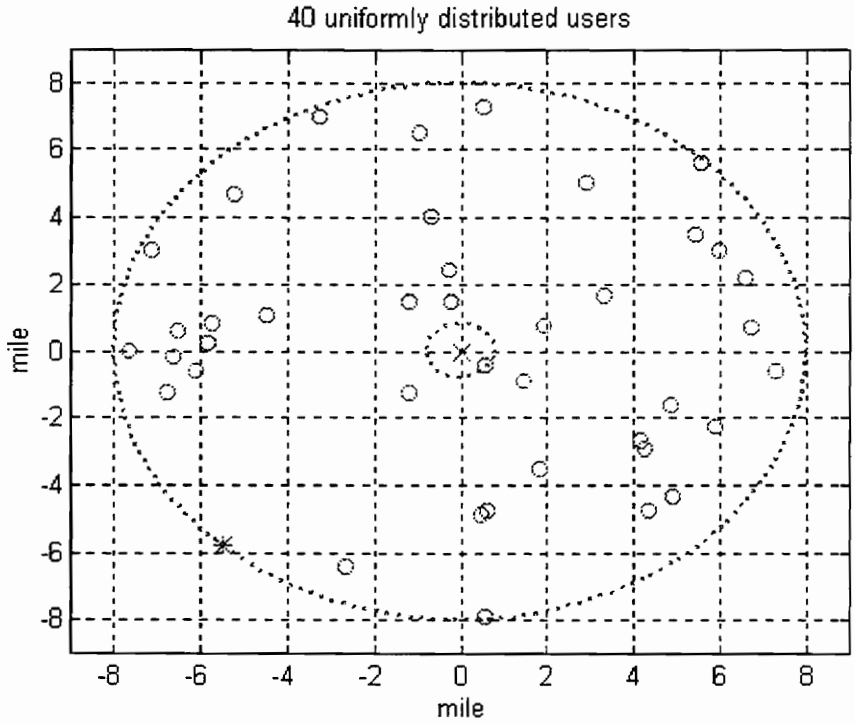

Figure 4.5.1 Uniformly distributed mobile units inside one cellsite coverage area

A typical bandwidth for a narrowband signal is 5 kHz and a typical modulation type is FM. CDMA systems that overlay on narrowband signals should be able to overcome this unintended jamming and provide a flexible means of using the spectrum.

TDAF processing of DS-SS signals allows correlated spectral energy to be utilized, even if the correlated spectral energy is corrupted by dissimilar interference. The energy from undesired signals is removed and replaced by a spectral correlated portion of the desired DS-SS signal components.

The geographical distribution of narrowband interference sources is modeled in Section 4.4. The narrowband interference-to-signal ratio J/S increases with the number of narrowband interference sources.

4.7 Model of multipath distortion

The time varying, or dynamic changes in the propagation path lengths, are related directly to the motion of the receiver. The rate of change of phase, due to motion, results in a Doppler shift for each propagation path. When a mobile unit moves with velocity v over a distance d in time interval Δt, the change in frequency (the Doppler shift) is given by

$$f_m = -\frac{1}{2\pi}\frac{\Delta\phi}{\Delta t} = \frac{v}{\lambda} \ . \tag{4.7.1}$$

Each multipath component experiences a different Doppler shift since the component arrives at the receiver at a different angle. The Doppler shift is related to the receiver speed as well as angle, α_i, of the i th component according to

$$f_i = f_m \cos\alpha_i \ , \tag{4.7.2}$$

where f_m is the Doppler frequency corresponding to a receiver speed v and a carrier wavelength λ. The expression for the received signal envelope is given by

$$S(f)=\begin{cases}\dfrac{E^2}{2\pi f_m\sqrt{1-\left(f/f_m\right)^2}} & f<f_m \\ 0 & f\geq f_m\end{cases}, \tag{4.7.3}$$

where E is the rms value of the signal envelope.

A received signal envelope can be represented by

$$S(t)=x(t)\cos\omega_c t-y(t)\sin\omega_c t=R\cos(\omega_c t+\theta), \tag{4.7.4}$$

where $x(t)$ and $y(t)$ are independent Gaussian processes and can be written as

$$x(t)=\sum A_i\cos(\omega_i t+\phi_i) \tag{4.7.5}$$

$$y(t)=\sum A_i\sin(\omega_i t+\phi_i), \tag{4.7.6}$$

where A_i, ω_i and ϕ_i are the amplitude, frequency, and phase of the i th component with its own Doppler shift. Since x and y are Gaussian random variables, the Rayleigh distributed envelope of the received signal is given by

$$R(t)=\sqrt{x^2(t)+y^2(t)}. \tag{4.7.7}$$

The phase of the received signal is given by

$$\theta = \tan^{-1}\frac{y(t)}{x(t)}, \tag{4.7.8}$$

and is uniformly distributed over $[0,2\pi)$. However, the change of phase is smooth and highly correlated over small distances.

Hence, it can be seen that the Rayleigh envelope can be generated from the Gaussian random processes and arriving Doppler shifted components are confined to the spectrum in Figure 4.7.1.

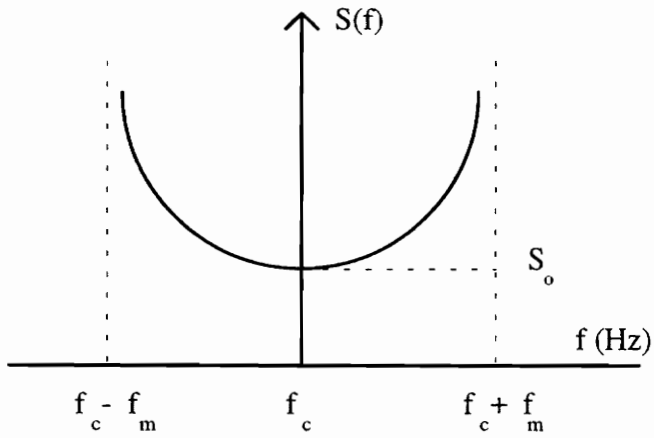

Figure 4.7.1 Theoretical spectrum of Rayleigh fading

In the computer simulations in Chapter 5, the Gaussian distributed random variables are obtained using a Gaussian number generator and each random variable is used as a Fourier coefficient. Each coefficient is weighted by a shaping factor obtained to the fading magnitude spectrum. The shaped fading magnitude spectrum, G(f) is represented by

$$G(f)=\begin{cases} r_f\left(1-\left(f/f_m\right)^2\right)^{-1/4} & 0\le f\le f_m-\delta f \\ r_f\left(f_m\left[\frac{\pi}{2}-\tan^{-1}\frac{(f-\delta f}{\sqrt{2f_m-\delta f}}\right]\right)^{1/2} & f=f_m \\ 0 & otherwise \end{cases} \tag{4.7.9}$$

where r_f is a Gaussian distributed random variable and $\left(1-\left(f/f_m\right)^2\right)^{-1/4}$ is the magnitude spectrum which is the square root of the power spectrum given in (4.7.9), and $\left(f_m\left[\frac{\pi}{2}-\tan^{-1}\frac{(f_m-\delta f)}{\sqrt{2f_m-\delta f}}\right]\right)^{1/2}$ is an estimate for the magnitude at f_m. Theoretically, the magnitude at f_m goes to infinity. In practice, the magnitude at f_m is estimated from the slope of the magnitude and the point $f_m-\delta f$. The magnitude spectrum is shown in Figure 4.7.2.

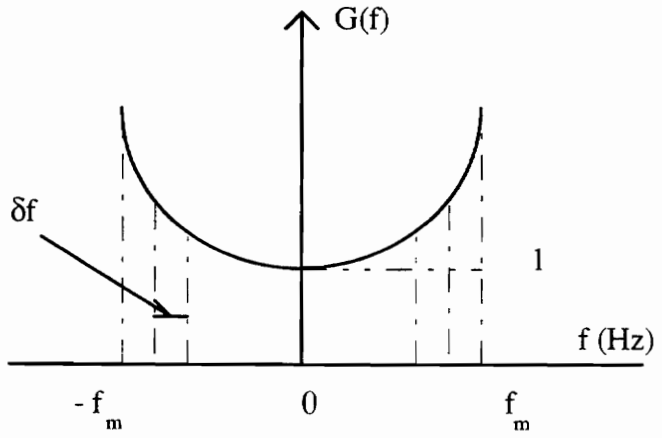

Figure 4.7.2 A spectrum of the fading signal envelope

A shaped spectrum $G(f)$ is generated for both the real part and the imaginary part of the received signal. Simply spectra are generated for the real parts and the imaginary parts of two Gaussian independent processes $x(t)$ and $y(t)$ as in (4.7.5) and (4.7.6). The real part is constrained to be an even function and the imaginary part is constrained to be an odd function. Hence, the real and imaginary outputs of the IFFT are two real Gaussian processes, which correspond to the time domain in-phase and quadrature part of the baseband fading signals in the time domain. The phase is uniformly distributed from 0 to 2π. The envelope and the phase generated are used as a time sequence to determine the amplitude and phase of the ray, respectively, in a particular channel as the receiver moves along a measured track.

The frequency selective fading is simulated by adding delayed signals. In urban areas, the delays tends to be shorter and relatively stronger than in rural areas.

Chapter 5

Simulation of AVM System Performance

5.0 Simulation parameters

In this chapter, the performance of the TDAF for DS-SS signals is evaluated. The system performance criteria are Bit Error Rate (BER) and Signal-to-Interference Ratio (SIR) at output. Constellation diagrams and spectrum plots are also used for evaluation. All simulations in this thesis are done on Sun Microsystems SPARC 5/10/20 workstations using the MATLAB 4.2 software and custom scripts. The signal parameters for the CDMA signals are listed in Table 5.0.1.

In order to maximize the performance of the conventional DS-SS demodulator, the 64 chip signature sequences employed in the simulations have characteristics similar to 63 chip Gold codes. For a preferred pair of maximal length sequences, 63 chip Gold codes can be generated with a maximum cross correlation of 15 chips for any arbitrary phase shift between separate code. However, for length 63 Gold code sequences there exist only two preferred generating polynomials. This means that the set of all possible signature sequences is limited to a total of 65 unique Gold codes. Such a low number of unique codes is clearly unacceptable for CDMA systems. By utilizing both preferred and

non-preferred generating polynomials, the maximum expected cross correlation is increased to 23 chips, but the available set of signature sequences becomes very large.

Table 5.0.1 System parameters in simulation

Modulation type:	DBPSK
processing gain:	64, or 18 dB
maximum data rate:	28.8 kbits/sec
chip rate:	1.8432 MHz
baseband bandwidth:	2 MHz
sample factor:	2 samples/chip
code repeat rate:	28.8 kbits/sec
samples per code repetition period:	128
FFT size:	128
Training sequence length:	200 data symbol
Training interval:	34.72 μs
Training time:	6.94 ms

A processing gain of 64 is used in the system, the first null-to-null baseband bandwidth is 1.8432 MHz. The spectral shaping filter introduced in Chapter 4 is used to reduce the magnitude of sidelobe. Any sidelobe peak greater than 2 MHz from the center frequency

is at least 26 dB lower than peak of the mainlobe. Notice that all the spectrum plots in this chapter are shown on normalized scale.

The TDAF structure is same as Figure 2.1.1. The code rate cycle frequencies for the DS-SS signals are spaced at multiples of

$$\alpha_{code} = \alpha_{data} = \frac{1}{T_{data}} = 28.8\ kHz \tag{5.0.1}$$

Notice that the sampling rate, chip rate, and code rate are integrally related. It is also useful to note that the required DFT size is a power of 2, thus, the computationally efficient FFT may be used in place of the DFT within the filter structure.

5.1 Narrowband FM interference

The basic ideal of CDMA overlay systems is to transmit DS-SS signals at a low level so that narrowband FM signals in the same spectrum experience only a slight increase in the received noise floor. TDAF processing of DS-SS signals can improve the tolerance of DS-SS to narrowband interference. In the ISM band, a pre-spreaded DS-SS signal will have not only multiple access interference but also narrowband interference from Part 15 devices. Although the FCC requires these narrowband signals to transmit at a low power, different propagation distances for each transmitter results in different RF path losses. The receive power of narrowband signals at base station varies significantly, and a high power

narrowband interference may jam the CDMA signals. This variation is referred to as the "near-far" problem.

To illustrate the advantages of TDAF processing for CDMA, a single DS-SS signal is corrupted by 10 narrowband FM signals as in shown in Figure *5.1.1*. The Signal-to-Interference Ratio (SIR) at output is shown in Figure 5.1.2. with variable the interference-to-signal power ratio J/S. E_b/N_o is either 10 dB or 20 dB. It can be seen that SIR slightly decrease with the J/S, when J/S becomes high.

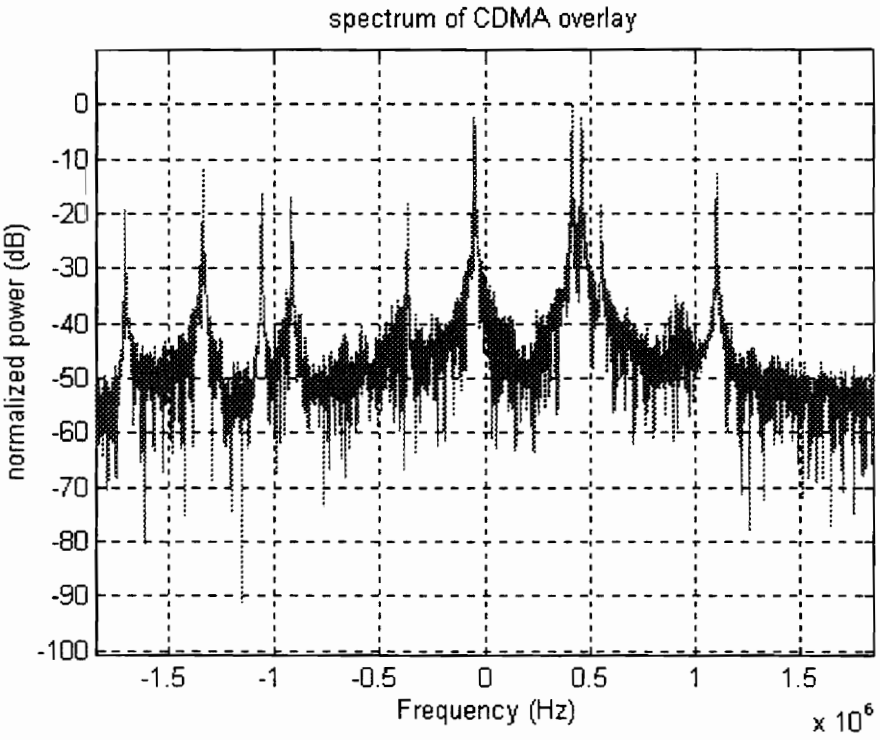

Figure 5.1.1 Spectrum of CDMA overlay on narrowband systems

TDAF processing can tolerate a high J/S of 45 dB and at the same time maintain a SIR over 20 dB. For comparison, notch filtering performance is also presented in the Figure 5.1.2, the number of taps is 128 and it has the same length as the TDAF. When J/S becomes large, the SIR at notch filter processing output decrease rapidly. Although there is no direct relationship between SIR and BER, the simulation indicates that the BER remains below 1×10^{-5} for J/S below 30 dB. The BER comparison is in Table 5.1.1. Viewed in the spectrum, the narrowband interference is too strong to be suppressed by the notch filter processing.

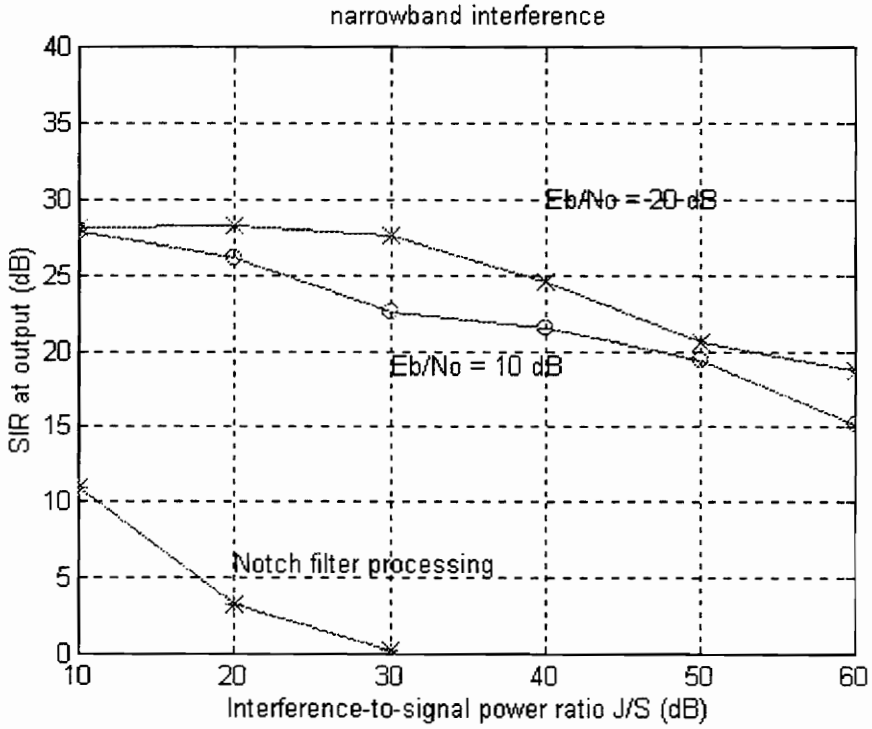

Figure 5.1.2 SIR at output versus J/S in narrowband FM interference environment

Table 5.1.1 BER comparison between TDAF and Notch filter processing

J/S	TDAF processing	Notch filter (N=128)
0 dB	$< 1\times10^{-5}$	6.19×10^{-3}
10 dB	$< 1\times10^{-5}$	2.16×10^{-2}
20 dB	$< 1\times10^{-5}$	8.1×10^{-2}
30 dB	$< 1\times10^{-5}$	$>1\times10^{-1}$

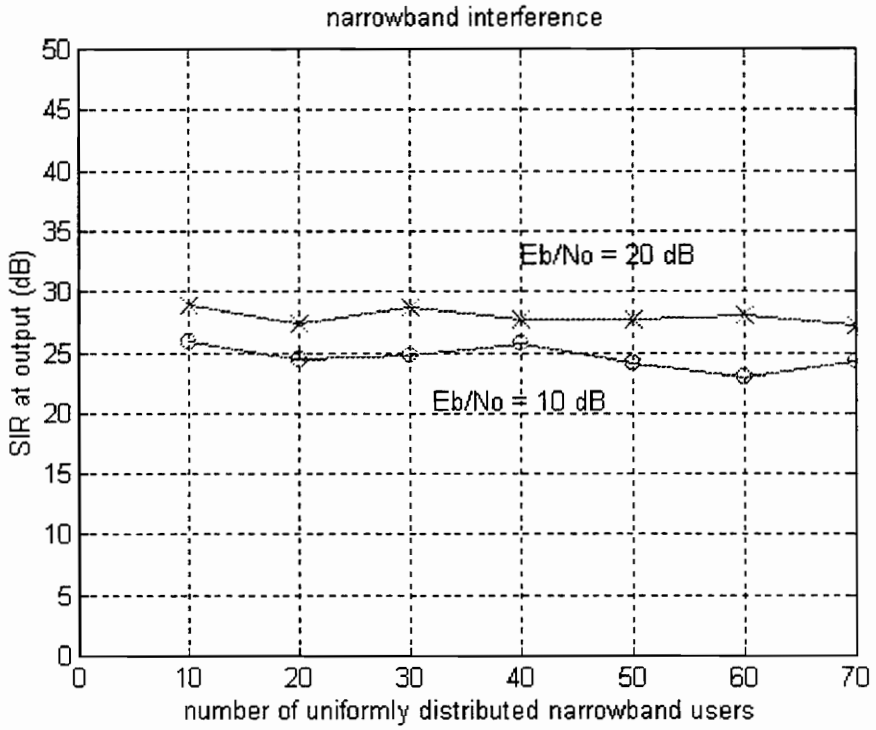

Figure 5.1.3 SIR at output versus number of simultaneous narrowband users

An appropriate model is to assume that FM users are uniformly distributed. The variation of received interference power caused by this statistical distribution of FM interference is presented in Section 4.4. Figure 5.1.3 demonstrates the SIR at output versus the number of narrowband FM interference users. The increases in the number the users who have uniformly distributed power levels does not cause a dramatic J/S increase; therefore, the SIR at output stays almost constant as the number of FM signals increases from 10 to 70.

Consider the case of narrowband interference, where there are 20 FM narrowband users, each with +40 dB higher power than the SOI, thus makes the J/S is 53.01 dB. Figure 5.1.4 shows the spectrum of the corrupted signal and Figure 5.1.5 shows the spectrum of the TDAF processed signal.

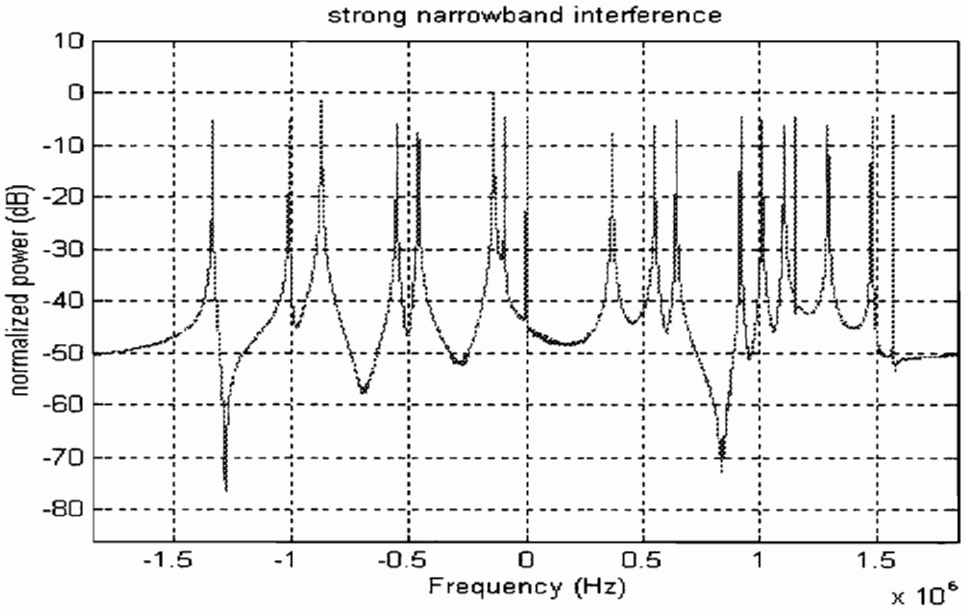

Figure 5.1.4 Spectrum of the received signal corrupted by strong narrowband interference

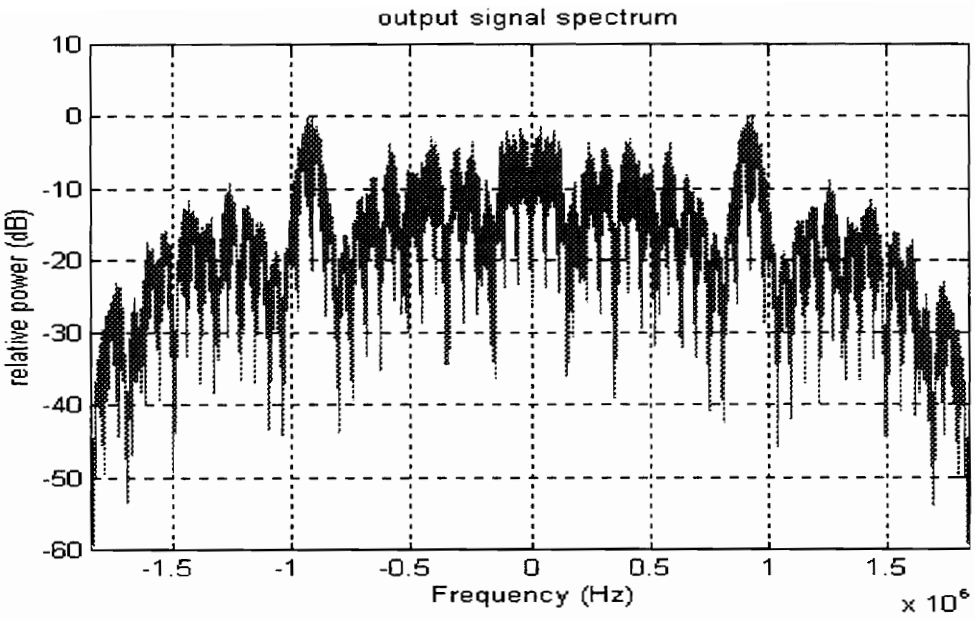

Figure 5.1.5 Spectrum of TDAF processed signal

This figure shows that TDAF processing has remove nearly all the narrowband interference. Figure 5.1.6 is the constellation diagram plot of TDAF processed signals. Note that there is only small variation of the symbols about the ideal states. The SIR at output is 17.35 dB.

The constellation diagram in Figure 5.1.7 presents the output for the notch filter. The 18 dB processing gain combined with notch filtering is insufficient to remove FM interference. Obviously, TDAF processing can achieve tremendous gain in interference tolerance compared to notch filtering and matched filter processing.

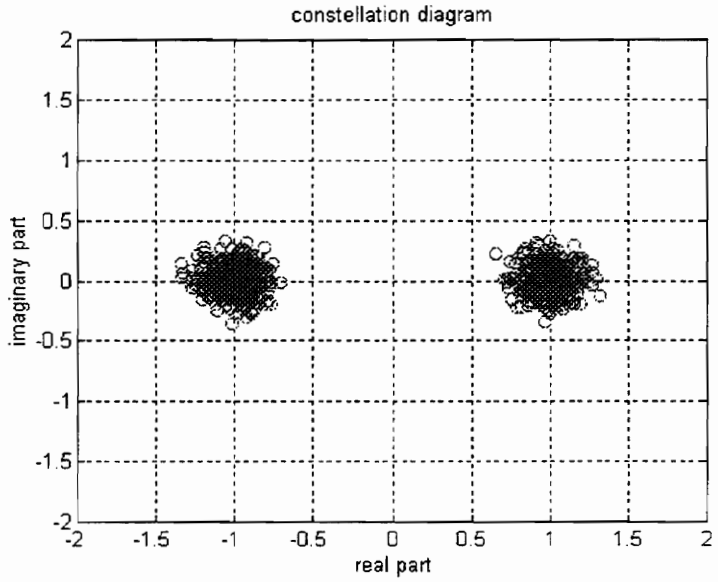

Figure 5.1.6 Constellation diagram of TDAF processed output signal

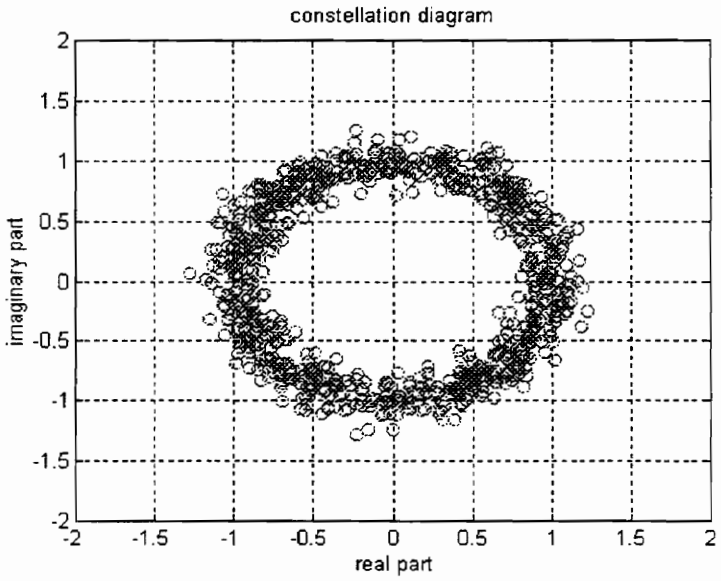

Figure 5.1.7 Constellation diagram of the notch and matched filter processed output signal

5.2 Adjacent channel interference

The proposed four sub-bands within the ISM band spectrum results in AVM systems locating their spectrum on the sidelobes of adjacent channels. Although, this partitioning can increase the number of available licenses, potential adjacent channel interference may cause degradation in system capacity. The spectral shaping filter was introduced in Section 4.3 to reduce the sidelobe effects. The spectrum of the CDMA before and after spectral shaping is presented in Figure 4.3.2 and Figure 4.3.3. Given a proper spectral shaping and equal power signals, the peak of the sidelobe leaking into the adjacent channel is at least -26 dB down from the peak of the mainlobe of the SOI.

RF propagation loss varies greatly from one user to another. Therefore the variance of base station receive power between a primary and an adjacent channel can be significant. Unfortunately, universal power control on all the users for different systems is not practical.

To demonstrate the effect of power variation of adjacent interference on system performance, a simulation is performed. It is assumed that the PN codes used in adjacent system are unknown random codes to the primary user. This means that the low cross-correlation and auto-correlation property are not guaranteed. Figure 5.2.1 is the spectrum of the primary user's CDMA signal. Figure 5.2.2 shows the CDMA signal corrupted by adjacent channel interference.

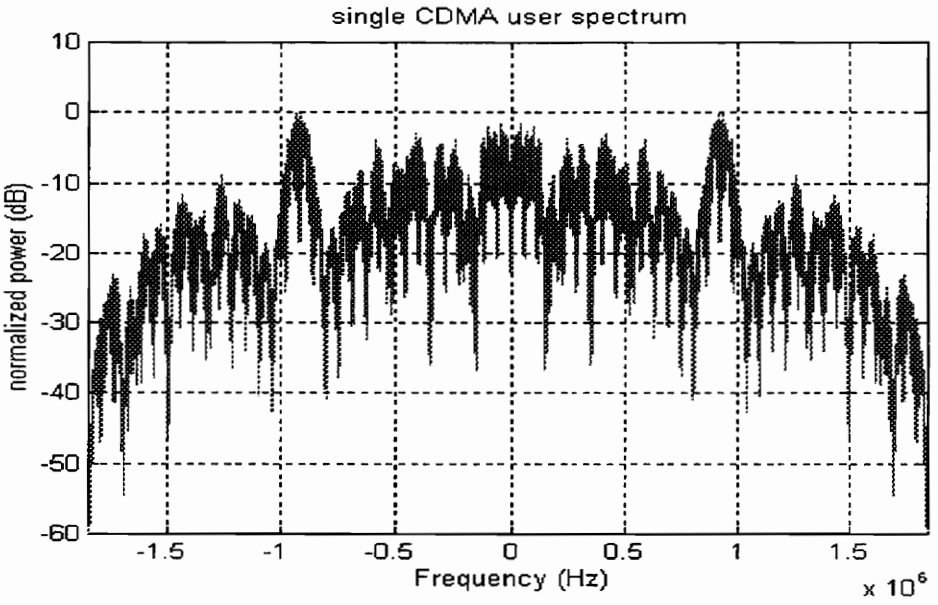

Figure 5.2.1 Spectrum of primary user's signal

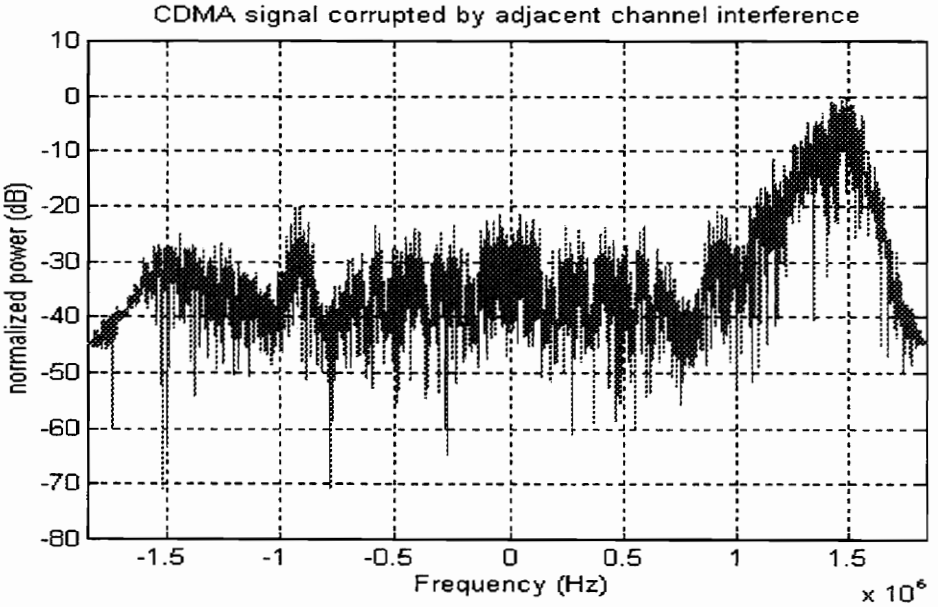

Figure 5.2.2 Spectrum of CDMA signal corrupted by adjacent channel interference

Figure 5.2.3 illustrates the SIR after the TDAF processing as a function of input J/S. There is only one user in the primary channel. The SNR in the primary channel is either 20 dB or 30 dB. The J/S is the ratio of the power of the 10 adjacent channel signals after spectral filtering to the power of the SOI after spectral filtering.

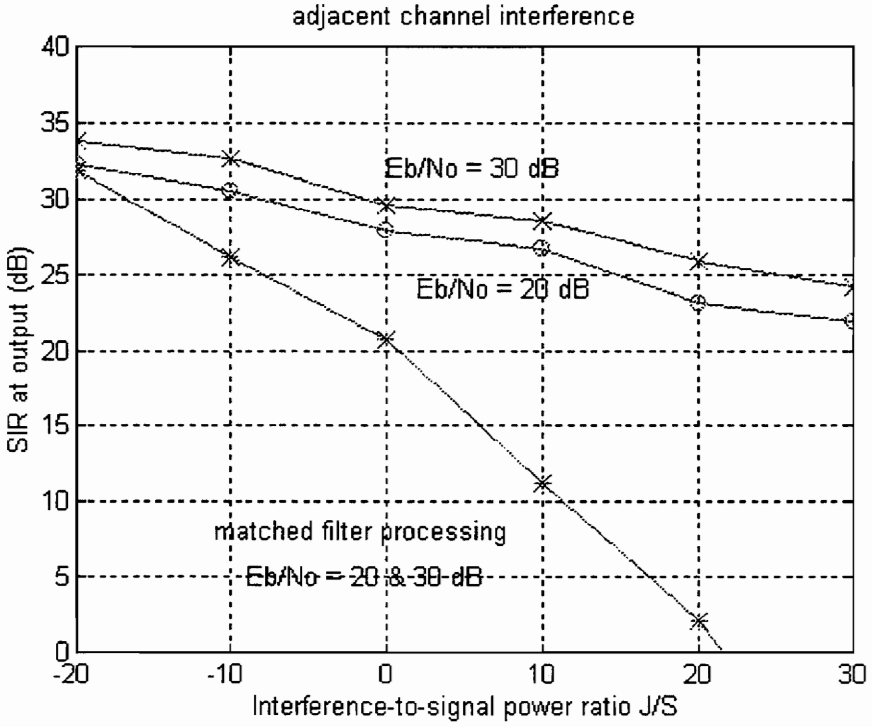

Figure 5.2.3 SIR at output versus J/S for an adjacent channel interference environment

Figure 5.2.3 shows that after TDAF processing, the SIR output for low J/S is very high. When $J/S > 0$, SIR decreases slowly with J/S. At a high J/S such as 30 dB, the SIR at output still remains over 20 dB. Overall, the BER for TDAF processed signals is much lower than the matched filter processed signal. The BER comparison is presented in Table 5.2.1. Generally, the SIR at the output of matched filter is highly sensitive to J/S. The

performances of both techniques are good when J/S is low. Compared with matched filter processing, TDAF processing has a much greater adjacent channel interference rejection capacity. The link budget can be improved by 15 dB when J/S is 10 dB.

Table 5.2.1 BER comparison between TDAF and matched filter processing

J/S	TDAF processing	matched filter
10 dB	$< 1\times10^{-5}$	2.16×10^{-4}
20 dB	$< 1\times10^{-5}$	8.1×10^{-2}
30 dB	$< 1\times10^{-5}$	$>1\times10^{-1}$

If the adjacent channel users are randomly located, the power level of each users can be calculated using the model introduced in Section 4.4. Figure 5.2.4 illustrates the SIR versus the number of uniformly distributed adjacent channel users. As the number of simultaneous adjacent users increases from 10 to 70, the corresponding J/S goes up by approximate 9 dB. TDAF processing can effectively reject the adjacent channel interference. With 70 adjacent channel users, the SIR at TDAF output remains over 28 dB. The SIR of the TDAF processed signal experiences a small increase when the number of simultaneous adjacent channel users goes up. Overall, the SIR of the TDAF output is significantly higher than that of matched filter output.

To emphasize prove the interference rejection power of the TDAF, an extremely strong adjacent channel interference scenario is simulated. Figure 5.2.5 shows the primary

an adjacent channels. There is a single user in the primary channel and 80 users operating in an adjacent channel with a total J/S of 25.78 dB. This might well represent the worst case of a fully loaded adjacent channel of an AVM system. Figure 5.2.6 illustrates the spectrum of the TDAF processed signal. The output spectrum is very close to the spectrum of the original signal spectrum shown in Figure 5.2.2.

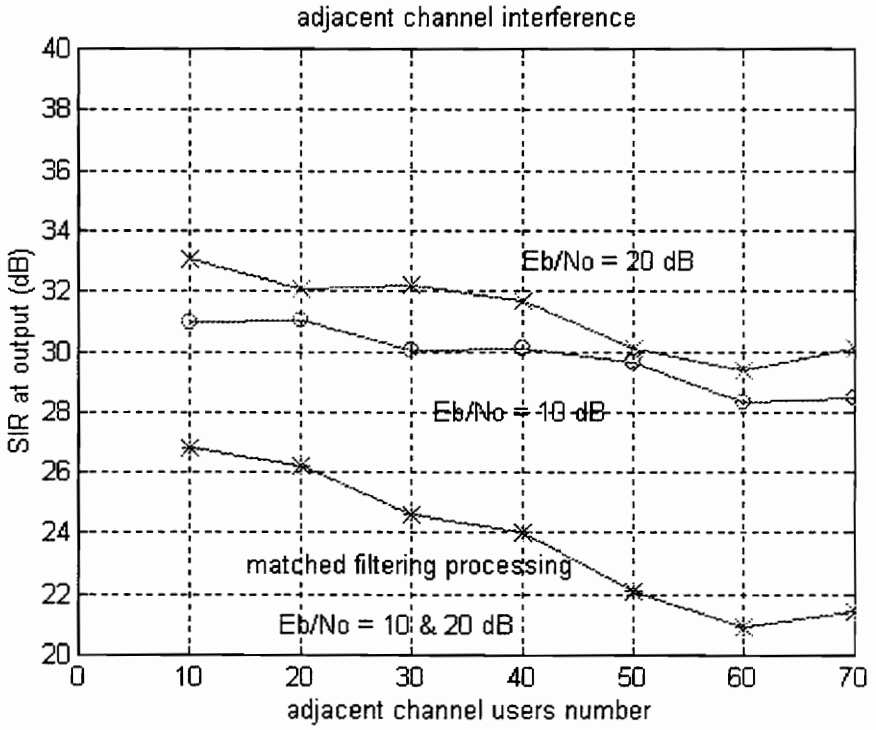

Figure 5.2.4 SIR at output versus number of adjacent channel users

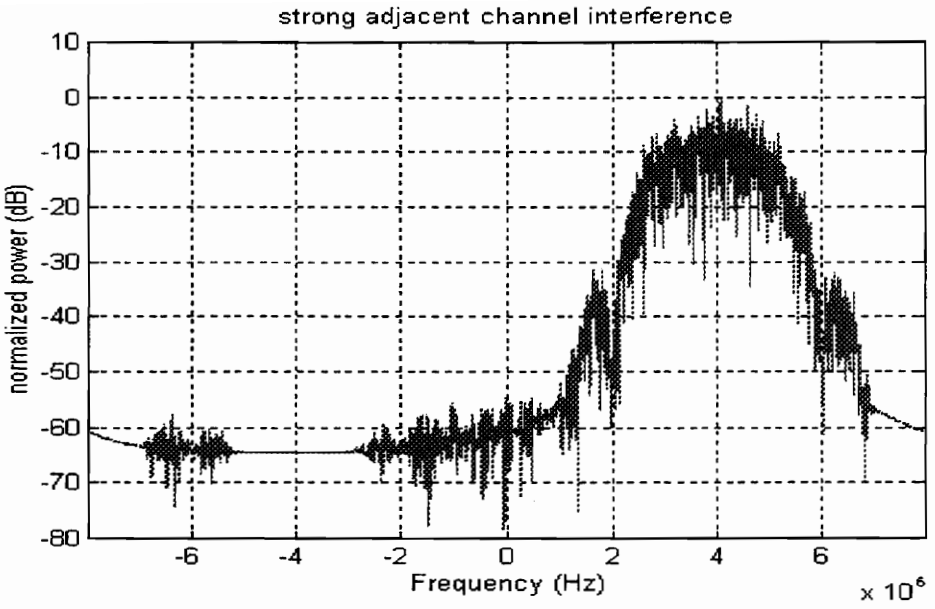

Figure 5.2.5 Spectrum of strong adjacent channel interference scenario

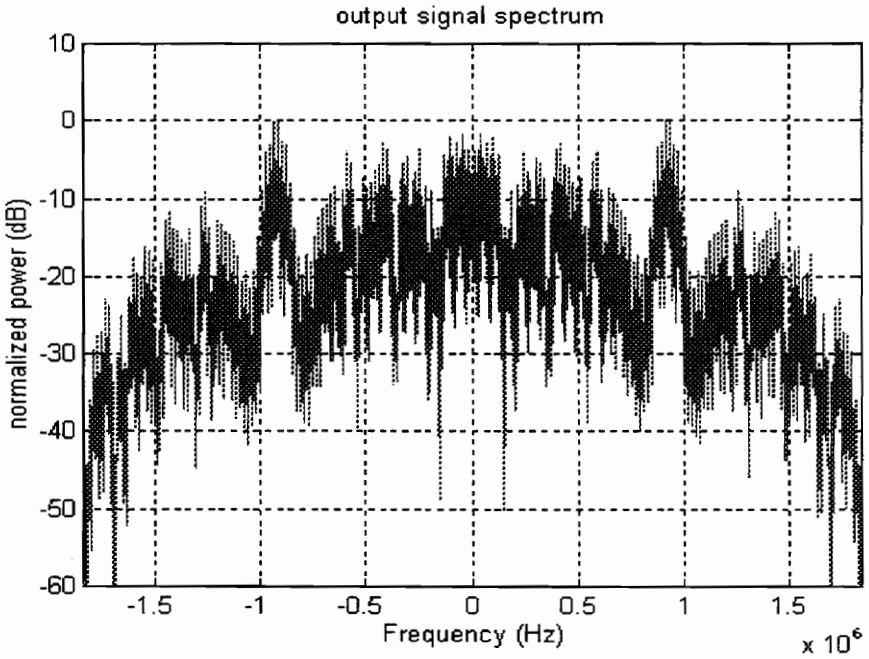

Figure 5.2.6 Spectrum of output signal after TDAF processing

For comparison, both the conventional matched filtered signal and TDAF processed signal constellation diagrams are shown in Figure 5.2.7 and Figure 5.2.8. The 18 dB processing gain of the DS-SS signal is clearly insufficient to combat the high level of interference. The SIR at output for matched filter processing signal is less than 0 dB. For TDAF processed signal, the SIR is 28.42 dB.

In summary, the use of TDAF processing and a spectral shaping filter can minimize the impact of adjacent channel interference. Even with extremely high adjacent channel interference, system performance is not significantly degraded.

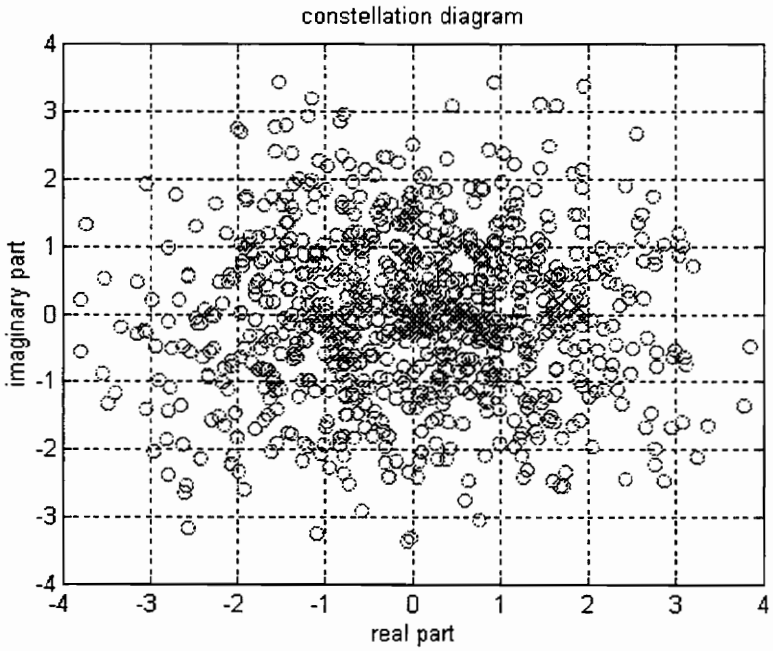

Figure 5.2.7 Constellation diagram for the signal after matched filter processing

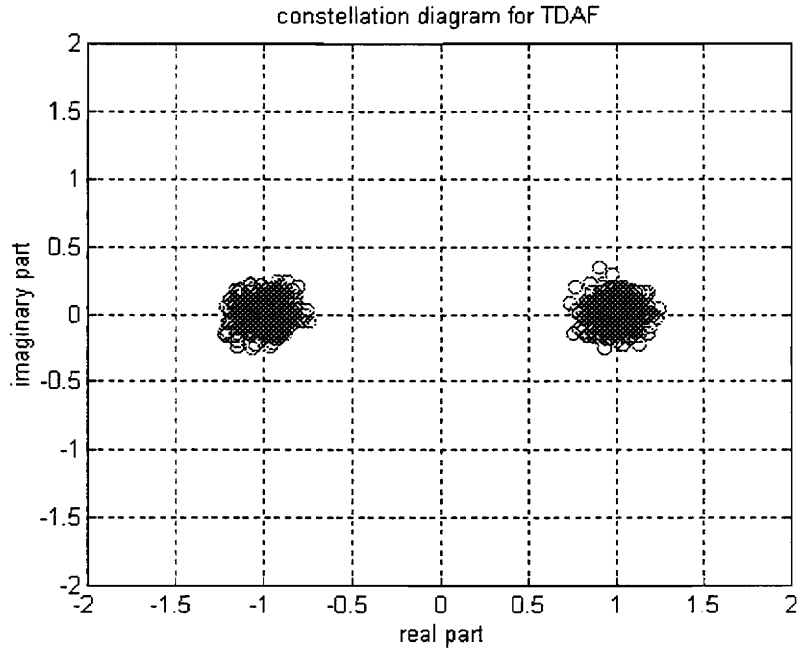

Figure 5.2.8 Constellation diagram for the signal after TDAF processing

5.3 Simulation for Rayleigh fading

A transmitted signal diffuses as it travels from the transmitter to the receiver. As a result, a portion of the transmitted signal's power arrives directly at the receiver while other portions of the transmitted signal's power arrive after being reflected from objects such as buildings, the ground, trees, leaves, people, etc. Thus, the transmitted signal takes multiple paths to the receiver and each path arrives after a different delay time with a different power.

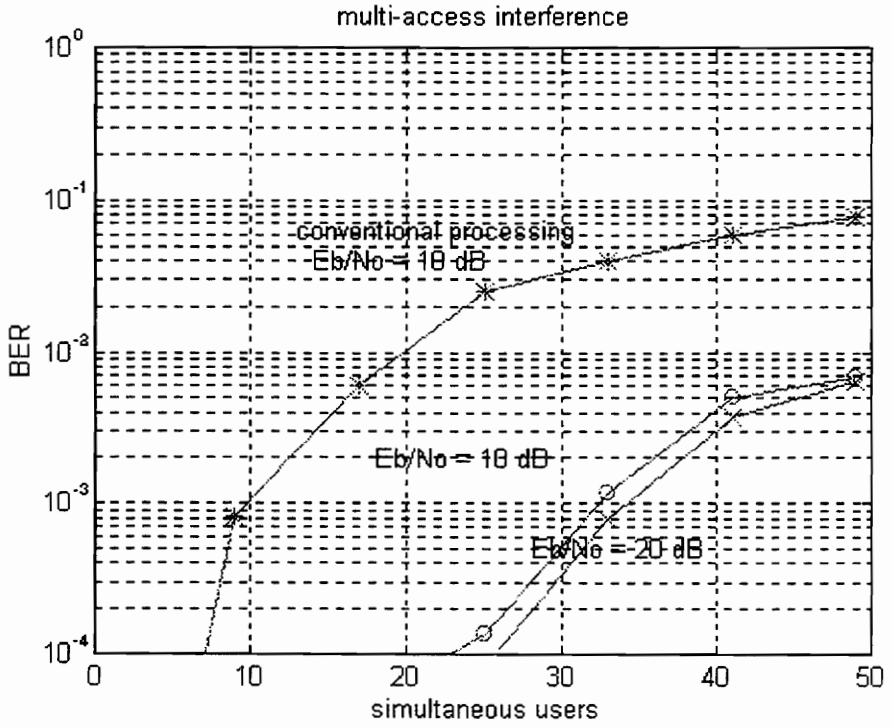

Figure 5.3.1 BER for TDAF processing with multi-access interference

For a baseline comparison, Figure 5.3.1 shows the TDAF performance in a multi-access interference environment with no fading. For comparison, the figure also shows the theoretical BER for the correlation receiver versus the number of simultaneous users assuming perfect power control and no fading. This analytical model was developed by Holtzman. The top curve in the plot shows the BER performance of the correlation receiver with a processing gain of 64 and a E_b/N_o of 10 dB. This curve is almost identical for E_b/N_o at 20 dB. The bottom curves represents average BER of TDAF processing, when E_b/N_o is 10 dB and 20 dB respectively. TDAF processing performs better than the conventional processing in a multi-access interference environment.

There are two types of fading involved in CDMA RF propagation, flat and frequency selective fading. If a mobile radio channel has a constant gain and linear phase response over a bandwidth which is greater than the bandwidth of the transmitted signal, then the received signal will undergo flat fading. Flat fading channels are also known as amplitude varying channels. In a flat fading channel the duration of a symbol is much large in time than the duration of spread of the channel impulse response. For this type of fading, the spectral characteristics of the transmitted signal are mostly preserved. The strength of the received signal will change with time, due to fluctuations in the gain of the channel caused by multipath; however, for the simulations perfect phase recovery is assumed.

Assuming that the fade remains constant for 30 data symbol, or 1.04 ms, a new channel is used for every 1.04 ms. The simulated BER performance as a function of E_b/N_o for DBPSK in flat fading channel is shown in Figure 5.3.2. The top curve represents

conventional processing with E_b/N_o = 20 dB. The bottom two curves represent TDAF processing with E_b/N_o of 10 dB and 20 dB, respectively. TDAF processing is clearly superior to conventional processing. The impact of E_b/N_o becomes less important when number of simultaneous uses goes up. The BER performance of the TDAF processing is much better than that of the matched filter. If a system has 25 simultaneous users and E_b/N_o is 20 dB, BER stays below 1×10^{-3} by using TDAF processing.

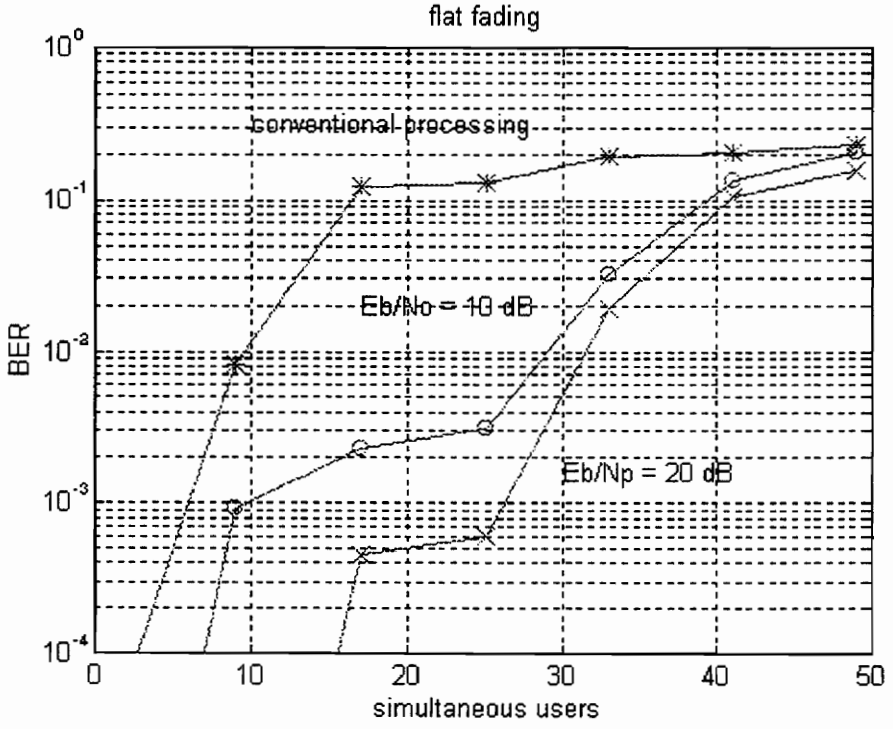

Figure 5.3.2 BER versus the number of simultaneous users (flat fading)

Figure 5.3.3 illustrates the effect of a vehicle speed on the system capacity. Vehicle speed varies from 0 km/hr to 120 km/hr. The middle curve represents the case which has 30 users and an E_b/N_o of 20 dB users. The BER goes up quickly with the vehicle speed

and remains steady for higher velocity. The overall BER for TDAF processing is much better than that of conventional filter processing.

If the channel has a constant gain and linear phase bandwidth that is much smaller than the bandwidth of transmitted signal, then the channel induces frequency selective fading. In this case, the channel impulse response has a multipath delay spread which is greater than the time duration of a chip. In this case, the received signal includes multiple versions of the transmitted waveform which are fading and delayed in time. Viewed in the

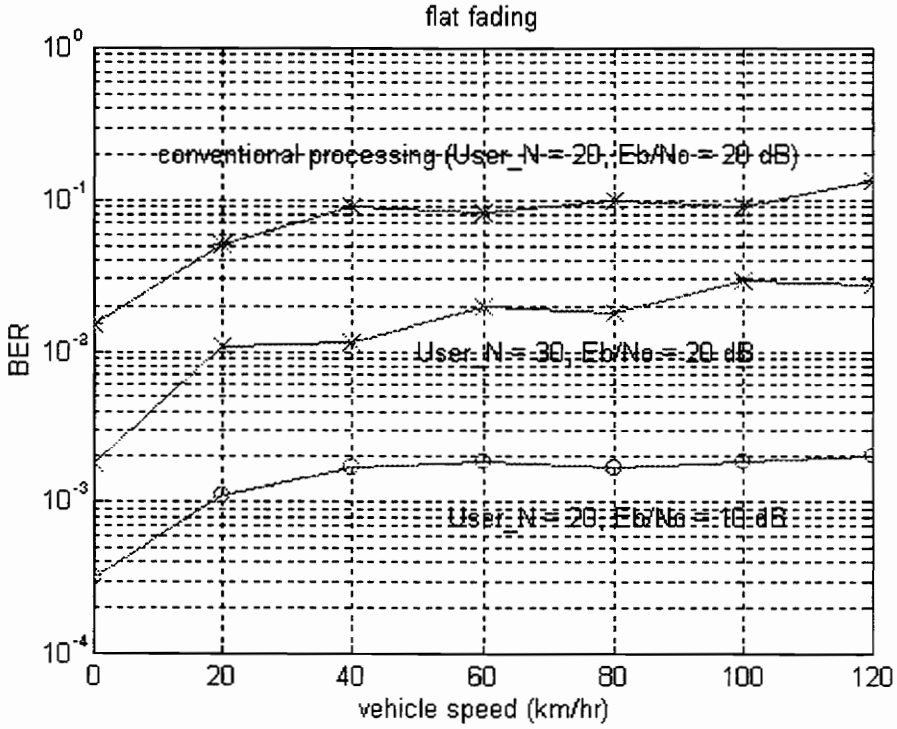

Figure 5.3.3 BER versus vehicle speed (flat fading)

frequency domain, certain frequency components in the received signal spectrum have a higher gain than others.

Urban and suburban areas have different frequency selective fading characteristics. In an urban area, the second path in the two-ray model tends to have a shorter delay and a stronger amplitude. However, in a rural area, the second ray tends to be longer and has a lower amplitude. The transmitted signal contains a high degree of spectral correlation, and the frequency selective fades occur at a frequency spacing greater than the interval of spectral correlation. The TDAF processing can correct the corrupted signal by replacing the portion of the attenuated spectrum by another portion enhanced by the multipath.

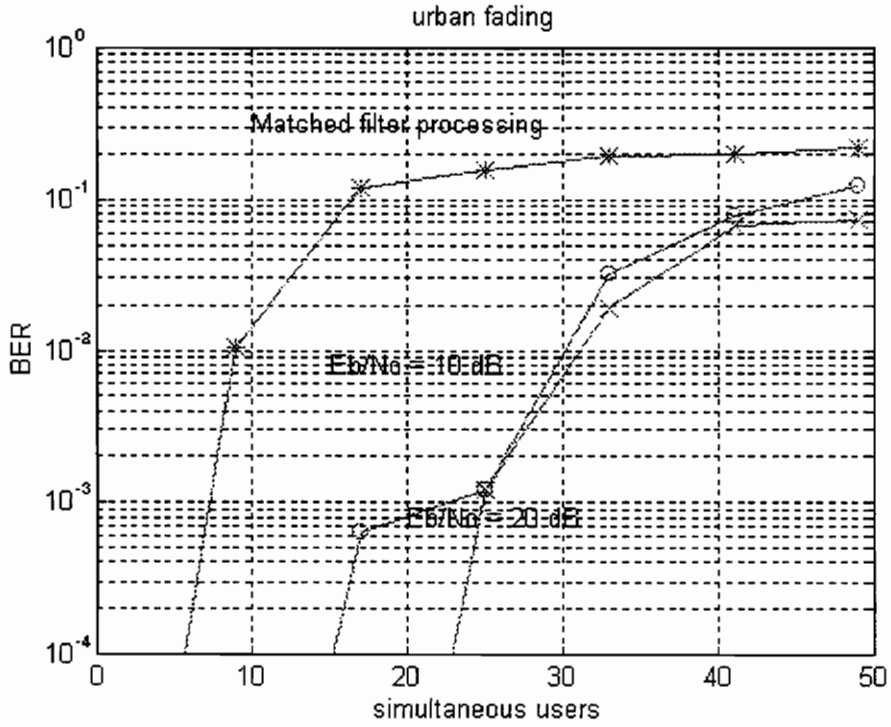

Figure 5.3.4 BER versus number of users in urban areas (frequency selective fading)

In the first example, a mobile unit operates in an urban area. It is assumed that delay of the indirect path is random and uniformly distributed in the range from 4 chip to 8 chip intervals. The average delay is 6 chip interval, or 3 microseconds. The attenuation on the amplitude of the second path is 6 dB. The fading pattern changes every 30 data symbols, or 1.04 ms. Figure 5.3.4 illustrates BER as a function of the number of simultaneous users. Again, all users are under perfect power control. With such strong fading, the BER for the match filter processing increases rapidly with the number of users. The BER of the TDAF processed signal is better. A BER tolerance of 1×10^{-3} can support about 25 simultaneous users. Comparing with Figure 5.3.1 in which no fading is presented, urban fading does not severely hurt the system performance if TDAF processing is used.

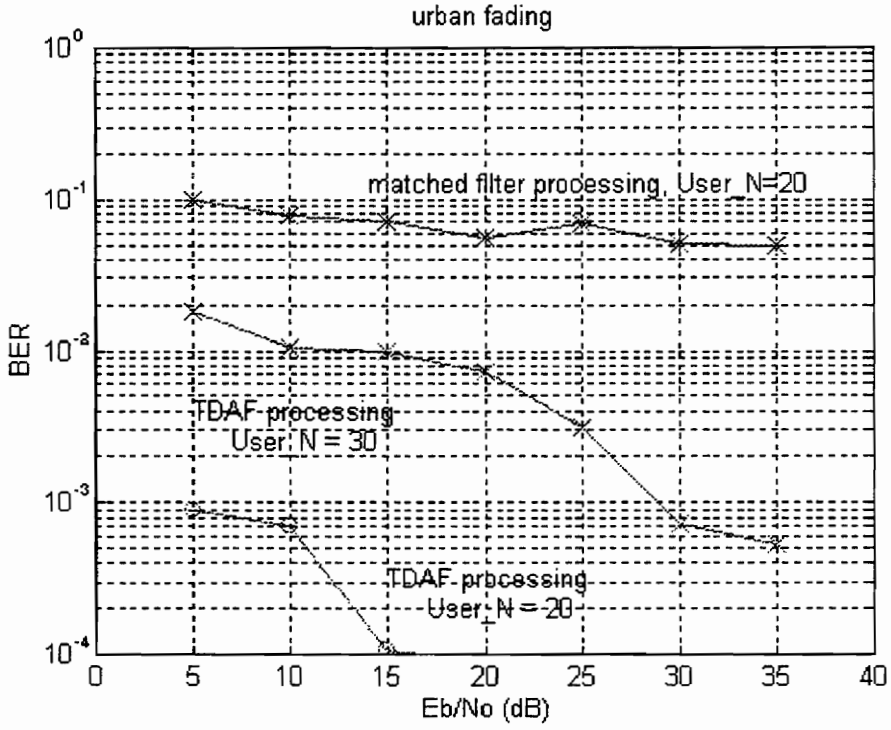

Figure 5.3.5 BER versus E_b/N_o in urban areas (frequency selective fading)

The Figure 5.3.5 shows the BER versus E_b/N_o. The bottom two curves represents the BER of TDAF processing with 20 and 30 simultaneous users, respectively. All users are under perfect power control. With 20 users in the system, the BER remains below 1×10^{-3} even for low E_b/N_o. Likewise, in a scenario with 30 users, it requires E_b/N_o greater than over 30 dB to have a BER less than 1×10^{-3}. Again, system capacity is significantly improved by the TDAF processing instead of the matched filter processing.

The performance in a rural area is simulated in the next example. The indirect path has a random delay uniformly distributed from 16 to 24 chips. The average delay is set at 20 chip intervals, or 10 ms, the attenuation of the second ray is 12 dB. Figure 5.3.6 illustrates the BER performance using TDAF processing and matched filter processing.

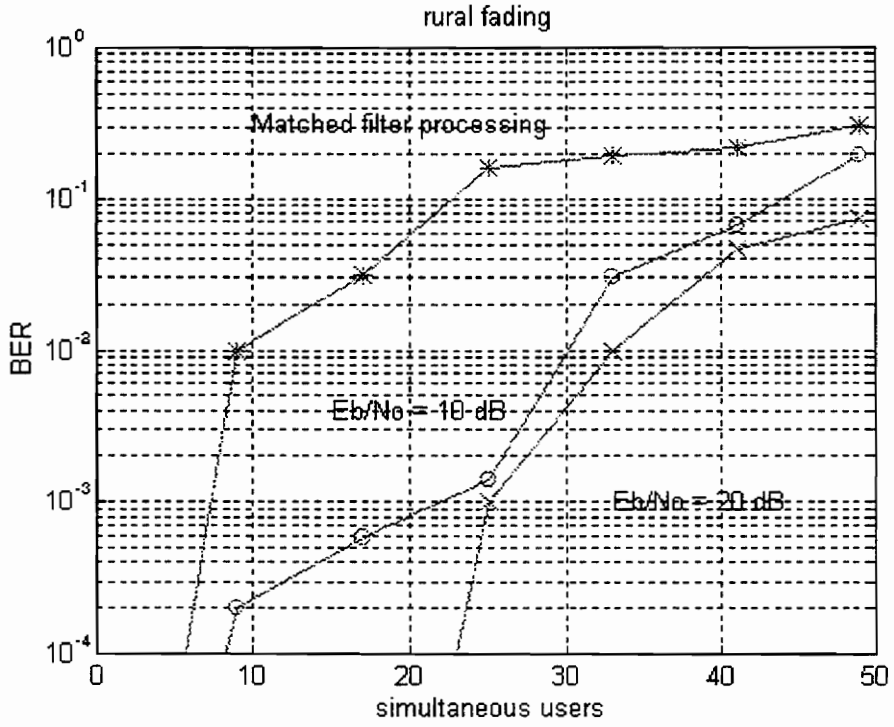

Figure 5.3.6 BER versus number of users in rural areas (frequency selective fading)

The results show that BER for TDAF processing is significantly lower than for matched filter processing. Using TDAF processing, a system with 25 simultaneous users and E_b/N_o higher than 10 dB, the BER is better than 1×10^{-3}.

Results in Figure 5.3.7 shows the BER versus E_b/N_o when the system has 20 or 30 simultaneous users. With 20 users in the system, the BER remains below 1×10^{-3} even if E_b/N_o is low. In a scenario with 30 users, E_b/N_o should be over 25 dB to have a BER less than 1×10^{-3}. The performances of the TDAF in urban and rural frequency selective fading environments are very similar.

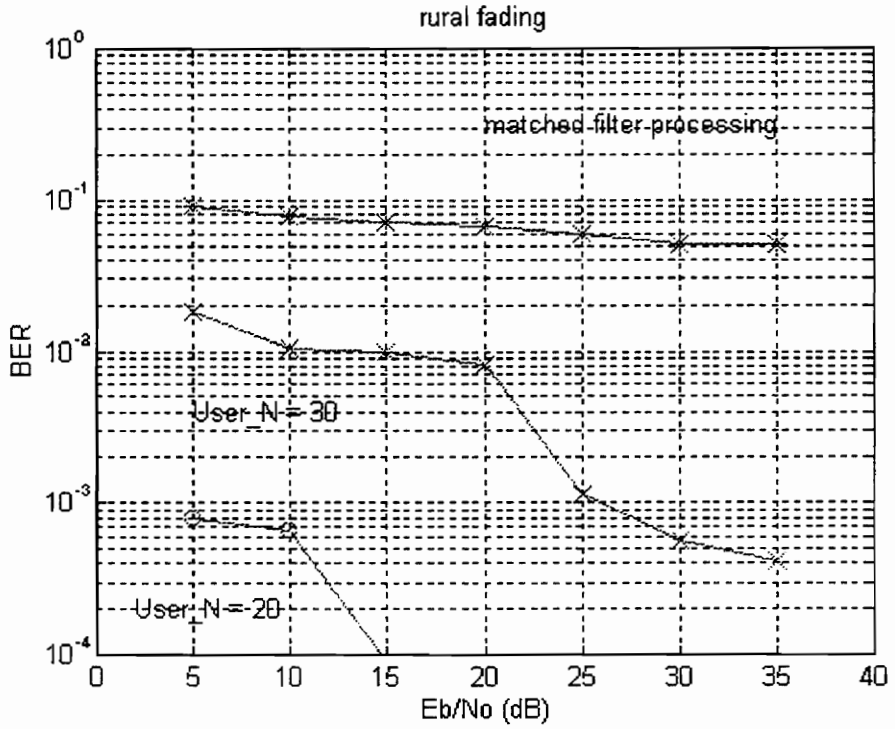

Figure 5.3.7 BER versus E_b/N_o in rural areas (frequency selective fading)

The TDAF can utilize energy of both the direct path and delay paths components. The effect is similar to the correction achieved by time diversity exploitation in the equalizer, since the TDAF is a generalization of an adaptive equalizer.

Chapter 6

Conclusions and Future Research

The purpose of this thesis is to show the utility of a Time Dependent Adaptive Filter (TDAF) in the universal digital receiver for CDMA Automatic Vehicle Monitoring (AVM) systems. It is also shown how multiple AVM service providers can exist in adjacent channels within the ISM band and realistic channel models for these system are also presented. It has been demonstrated that the TDAF can provide substantial improvement in interference rejection over the conventional correlation receiver. The performance is described using SIR and Bit-Error-Rate (BER) measurements. Computationally effective TDAF structures have been proposed to handle the case of different code repeat intervals for the different systems.

6.1 Summary of results

For the ISM band CDMA AVM systems, direct overlay of different AVM systems in the same frequency band depends on power control among all users; however, universal power control does not seem to be practical. Partial overlay systems are feasible, i.e., it is possible to locate the mainlobe of one AVM system over a sidelobe of a second system. Therefore, a spectral shaping filtering is required before transmission to reduce adjacent channel interference level.

The TDAF requires no knowledge of the other users in the system in order to produce marked increases in user capacity and can be configured to handle various modulation format. BER and SIR at output simulations have shown that TDAF is able to mitigate many different forms of interference common to the mobile channel. First, in a scenario with strong narrowband FM interference, it can be seen that SIR tends to slightly decrease with increasing J/S. The TDAF processing can tolerate a high J/S of 45 dB and maintain a SIR over 20 dB. If it is assumed that a large number of narrowband users locations are uniformly distributed, the interference may not have any significant impact on the CDMA BER. The performance gain provided by the TDAF processing is much better than traditional notch filter processing.

Second, in an adjacent channel interference environment, the SIR at output of the TDAF remains insensitive to low input J/S. It appears that impact of adjacent channel on SIR only slightly increases when J/S is over 0 dB. Even with a J/S of 30 dB, TDAF processing can still effectively remove the adjacent interference. With 70 adjacent channel simultaneous users, whose locations have an uniform distribution, the SIR stays above 20 dB.

The TDAF can utilize energy of both direct path and delay paths components. The effect is similar to the correction achieved by time diversity exploitation in the equalizer, since the TDAF is a generalization of an adaptive equalizer.

The implementation of RLS algorithm gives TDAF a fast convergence speed and a low steady-state mean square error. These features make the TDAF highly attractive for the ISM band AVM systems.

A mixture of signals with different code repeat rates is possible. Long FFT and switching long FFT architectures provide an approach to mitigate multi-access interference with different code repeat rates. However using these architecture TDAF processing requires accurate synchronization. Imperfect synchronization may result inconvergence or mistracking in TDAF processing.

6.2 Future research

In this study, perfect phase recovery and synchronization have been assumed. In practice, the phase lock loop can not guarantee accurate phase tracking. The sensitivity of TDAF performance to this phase error is unknown. In the multi-access interference simulation, different users' signals are assumed to have perfect time alignment; however, the impact of asynchronization drift needs to be examined.

Another interesting topic is overlaying of CDMA systems with different code repeat rates. The primary user has to combat with multiple access interference not only from its own system, but also from signals with different code repeat rate. Different code intervals that do not share a common integer related code repeat intervals to allow for the use of a switching or long FFT structure can be a significant degradation of system performance.

Exploitation of cyclostationarity for signal detection and estimation via its associated spectral correlation usually requires detailed knowledge of the cycle frequencies of the signals. One solution is to provide extremely fine channelization of the signal so that the bin centers of channelizer closely approximate multiples of the fundamental cycle frequencies.

Appendix A

Reference

[Abj92] M. Abjulrahuman, D.D.Falconer, and A.Sheikh, "Equalization for interference cancellation in spread spectrum multiple access systems," *Proceedings VTC*, May 1992.

[Age93] B.G. Agee, "Solving the near-far problem: Exploitation of spatial and spectral diversity in wireless personal communications networks", *Proceedings of the Third annual Symposium on Wireless Communications*, vol. 1, p.15-1, 15-1, Mobile and Portable Radio Research Group, Virginia Tech, June, 1993.

[Aue94] V.Aue, "CDMA interference rejection using a radial basis function neural net," *Master's thesis*, Mobile and Portable Radio Research Group, Virginia Tech, January, 1994.

[Bue94] R.M.Buehrer and B.D.Woerner, 'Spread spectrum for wireless communications," *Proceedings of Fourth Symposium on Wireless Personal Communications*, p.1-1,1-27, Mobile and Portable Radio Research Group, Virginia Tech, June, 1994.

[Bul77] K. Bullington, "Radio propagation for vehicular communications", *IEEE Transactions Veh. Technol.*, vol. VT-26, no.4, page 295-308, Nov, 1977.

[Che88] Chihkang Chen, "*Spectral correlation characterization of modulated signals with application to signal detection and source location*". Ph.D. Dissertation, Department of Electrical and Computer Engineering, UC at Davis, 1988.

[Cro83] R.E.Crochiere, L.R.Rabiner, "*Multirate Digital Signal Processing*," Prentice-Hall, Englewood Cliffs, NJ, 1983.

[Dix84] Robert C. Dixon, "Spread Spectrum Systems. John Wiley and Sons, New York, second edition, 1984.

[DMW78] M.Dentino, J.McCool, and B.Widrow, "*Adaptive filtering in the frequency domain*," Proceeding of the IEEE, vol.66, p. 1658-1659, December, 1978.

[Fer85] E.Ferrara, "*Frequency domain implementations of periodically time varying filters*", IEEE Transactions on Acoustics, Speech, and Signal Processing, ASSP-33, p. 883-892, August, 1985.

[Feu94] M. Feuerstein, G. Clausius, D. Vendetti, "Design and test of CDMA cellular systems", In *Proceedings of the 1994 IEEE Vehicle Technology Conference*, volume 1, pages 6-10. IEEE Vehicular Technology Society, 1994.

[Fun91] Victor Fung, "Bit Error Simulation of FSK, BPSK, and $\pi/4$ DQPSK in Flat and Frequency Selective Fading Radio Channels using Two-Ray and Measurement-Based Impulse Response Models, unpublished master's thesis, Mobile and Portable Radio Research Group (MPRG-TR-91-12), Bradley Department of Electrical Engineering, Virginia Tech, august 27, 1991.

[Gar85] W.A.Gardner, "Introduction to Random Processes with Applications to Signals and Systems," MacMillan, New York, 1985.

[Gar87a] W.A.Gardner. "Spectral correlation of modulated signals: Part I - analog modulation," *IEEE Transactions on Communications*, COM-35: 584-594, June, 1987.

[Gar87b] W.A.Gardner, William A. Brown, and Chih Kang Chen. "Spectral correlation of modulated signals: Part II- digital modulation," *IEEE Transactions on Communications*, COM-35: p.595-601, June, 1987.

[Goo91] D.J.Goodman, "Second generation wireless information networks," *IEEE Transaction on Vehicular technology*, vol.40, p.366-374, May, 1991.

[Hen93] F.Hendessi, H.M.Hafez, and A.U.Sheikh. "The structure and performance of fresh decision feedback equalizer in the presence of adjacent channel interference," *Proceedings of 43rd IEEE Vehicular Technology Conference*, p.641-644, Secaucus, New Jersey, May, 1993.

[Hol91] J.M.Holtzman, "A simple accurate method to calculate spread spectrum multiple access error probabalities," *Proceedings of the IEEE International Confereence on Communications*, vol.3 pp. 1633-1636, Denver, June, 1991.

[Hol93] R.D.Holley and J.H.Reed, "Time dependent adaptive filters for interference cancellation in CDMA systems," unpublished master's thesis, Mobile and Portable Radio Research Group (MPRG-TR-93-15A), Bradley Department of Electrical Engineering, Virginia Tech, October, 1993.

[Hua91] W.Huang and T.S.Rappaport, "A competitive study of two adaptive equalizers for mobile radio," *Proceedings of the 1991 IEEE Vehicular Technology Conference*, p.765-769, IEEE Vehicular Technology Society, May, 1991.

[Itl78] R.A. Iltis and L.B. Milstein, "Performance analysis of narrowband interference rejection techniques in DS spread spectrum systems," *IEEE Trans. Comm.* vol. COM-26, page 209-216, Feb, 1978.

[Jer92] M.C.Jeruchim, P.Balaban, K.S.Shanmugan, "*Simulation of Communications Systems*", Plenum Press, New York, 1992.

[Las94] J.D.Laster and J.H.Reed, "A survey of adaptive single channel interference rejection techniques for wireless communications," *Proceedings of Fourth Symposium on Wireless Personal Communications*, p.1-1,1-27, Mobile and Portable Radio Research Group, Virginia Tech, June, 1994.

[Li93] Y.Li, "Bit error rate simulation of a CDMA system for personal communications," Master's thesis, Mobile and Portable Radio Research Group, Virginia Tech, July, 1993.

[Mad93] U. Madhow and M.L. Honig, "Minimum mean squared error interference suppression for direct-sequence spread-spectrum code-division multiple-access," *ICUPC '92 Proceedings*, September, 1993.

[Mil86] L.B.Milstein and R.A. Itis, "Signal processing for inference rejection in spread spectrum communications", *IEEE ASSP Magazine*, p.18-31, April, 1986.

[Mon93] P.N.Monogioudis, R. Tafazolli, and B.G. Evans, "Linear adaptive fractionally spaced equalization of CDMA multiple-access interference," *Electronics Letters*, vol.29, no.21, page 1823-1825, October, 1993.

[MPG92] R.S.Mowbray, R.D.Pringle, and P.M.Grant, "Increased CDMA system capacity through adaptive cochannel interference regeneration and cancellation", *IEE Proceedings - I*, vol. 139, p.515-524, October, 1992.

[MRH89] R.Mendoza, J.H.Reed, and T.Hsia, "Interference rejection using a hybrid constant modulus algorithm and spectral correlation discriminator," *1989 IEEE Military Communications Conference Proceedings*, Boston, October, 1989.

[Opp89] A.V.Oppenheim, R.W.Schafer, "*Discrete-Time Signal Processing*", Prentice Hall, Englewood Cliffs, New Jersey, 1989.

[Par93] J.D.Parsons, "*The Mobile Radio Propagation Channel*", Halsted Press, 1993.

[Rap92] T.S.Rappaport, L.B.Milstein, "Effects of radio propagation path loss on DS-CDMA cellular frequency reuse efficiency for the reverse channel," *IEEE Transactions on Vehicular Technology*, vol.41, p.231-241, August, 1992.

[Rap94] T.S.Rappaport and S.Sandhu, "Radio wave propagation for emerging wireless personal communication systems", *Proceedings of Fourth Symposium on Wireless Personal Communications*, p.1-1,1-27, Mobile and Portable Radio Research Group, Virginia Tech, June, 1994.

[Ree87] J.H.Reed, "Time dependent adaptive filters for interference rejection," Ph.D. Dissertation, Department of Electrical Engineering and Computer Engineering, University of California at Davis, December, 1987.

[Ree89] J.H.Reed, I.Howitt, V.Vermuri, and T.Hsia, "Recent developments in applying neural nets to equalization and interference rejection. In Proceedings of the Third Annual Symposium on Wireless Communications, vol. 1, p. 1-1, 1-12, Mobile and Portable Radio Research Group, Virginia Tech, June, 1993.

[Ree90] J.H.Reed, "The performance of time-dependent optimal filtering for interference rejection," *IEEE Transactions on Signal Processing*, p.1373-1385, July, 1991.

[Sal92] A.Salmasi, "CDMA development status for digital cellular and personal communications network," *Proceedings of Second symposium on Wireless Personal Communications*, p.1-1, 1-15, Mobile and Portable Radio Research Group, Virginia Tech, June, 1992.

[Sch91] D.L.Schilling, L.B.Milsein, R.L.Pcikholtz, "Broadband CDMA for personal communications systems', *IEEE Communications Magazine*, p.86-93, Nov, 1991.

[Sch93] D.L.Schilling, G.R.Lomp, and J.Garodnick, "Broadband-CDMA overlay," *Proceedings of the 43rd IEEE Vehicular Technology Conference*, p.452-455, 1993.

[Shy92] J.J.Shynk, "Frequency domain and multirate adaptive filtering," IEEE Signal Processing Magazine, vol.9, p. 14-37, January, 1992.

[Var88] M.K.Varanasi and B. Aazhang, "An iterative detector for asynchronous spread spectrum multiple-access systems," *Proceedings of the IEEE Global Telecommunications Conference and Exhibition*, vol. 1, page 556-560, IEEE Communications Society, Nov., 1988.

[Var90] M.K.Varanasi and B. Aazhang, "Multistage detection in asynchronous code-division multiple-access communications," *IEEE Transactions on Communications*, vol. 38, p.509-519, April, 1990.

[Ver94] Sergio Verdú, "Adaptive multiuser detection," *Proceedings of IEEE third International Symposium on Spread Spectrum Techniques and Applications*, page 43-50, Oulu, Finland, 1994.

[Wan92] J.Wang and L.B.Milstein, "Applications of suppression filters for CDMA overlay situations," *Proceedings of 1992 International Conference on Communications*, p.310.3.1-310.5, June, 1992.

[Whi93] D.P.Whipple, "The CDMA Standard," *Applied Microwave And Wireless*, Winter, 1993, p.24-37..

[Woe92] B.D.Woerner and R.Cameron, "An analysis of CDMA with imperfect power control," *Proceedings of IEEE Vehicular Technology Conference*, May, 1992.

Appendix B

MATLAB Script

```
% TDAF processing program
% September 27, 1994


clear;
clg;


L_train=120;                    % training data sequence length
L_part=90;                      % data generation periodicity
L = 100*L_part                  % total data processed


fft_n = 128;                    % FFT size

chips  = 64;                    % Signal-of-interest code repeat rate
chips2 = 48;                    % SNOI_1 code repeat rate
chips3 = 48;                    % SNOI_2 code repeat rate

orders  = 2*chips;              % Signal-of-interest code block length
orders2 = 2*chips2;             % SNOI_1 code block length
orders3 = 2*chips3;             % SNOI_2 code block length

User_N=10;                      % total users in the same system
User_b=0;                       % SNOI_1 co-channel users
User_c=0;                       % SNOI_2 co-channel users
User_a = User_N-1;

N=orders*L;                     % total sample points
data_rate=28800;                % original data rate
sample_rate=data_rate*orders;   % sample rate

adj_User_N=0                    % adjacent channel users
FM_n=10;                        % FM interference sources
```

```
SNR=20;                          % signal-to-noise ratio
speed_km=40;                     % vehicle speed

Nearfar_max=50;                  % maximum near-far power (dB)
power_ray2 = -7;                 % attenuation for second ray
path2 = 40;                      % delay interval for second ray

coverage_mi = 8;                 % cellsite coverage radius

%  adj_power_dB = 10*ones(adj_User_N,1);
   adj_power_dB = nearfar(coverage_mi,adj_User_N);        % adjacent users' nearfar power level

   FM_carriers=sample_rate*fix(80*(rand(FM_n,1)-0.5))/80;  % FM carriers set
   FM_carriers=fix(FM_carriers/1000)*1000;

%                                   FM_amp_dB = 30*ones(FM_n,1);
   FM_amp_dB = nearfar(coverage_mi,FM_n);                 % FM users' nearfar power level

   doppler_shift = 900e6*(speed_km*1000/3600)/3e8;        % doppler shift frequency
   maxshift= fix(doppler_shift);


   ii=0;
   jj=0;

   train_error=0;
   total_error=0;
   blind_error=0;


%              .....................................................................

%              .      TDAF Processing with training sequence        .

%              .....................................................................


%  Weights adjustment when short training data sequence available


   W = zeros (fft_n);
   R = 10^4*eye(fft_n);
   Rho=1;
```

```
    step=1/8;                          % smooth factor
    scale=1;                           % output amplitude adjustment index

    MSE_adj(1,1) = 1;                  % smoothed MSE at output
    MSE_real_adj(1,1) = 1;             % smoothed MSE for real part at output


  for ii=1:L_train

    if  (ii-1)/L_part==fix((ii-1)/L_part)

      gen_data;                        % generation data periodically

    end;


    pos=ii-fix((ii-1)/L_part)*L_part;
    k_low=(pos-1)*orders+1;
    k_up =pos*orders;

    input_sample = channel(k_low:k_up,1);
    ideal_sample = ideal_data(ii,1)*ref_code;
    Xin = fft(input_sample,fft_n);
    Yin = fft(ideal_sample,fft_n);

    Yest=W*Xin;

    d_out = ifft(Yest,orders);         % using IFFT back to time-domain
    y_out = d_out.*ref_code;           % despreading

    diagram_out(ii,1) = sum(y_out)/orders;
    constell_out(ii,1)= diagram_out(ii,1);

%   AGC control

    scale=abs(diagram_out(ii,1))*step+(1-step)*scale;
    diagram_out(ii,1) = diagram_out(ii,1)/scale;
    final_data(ii,1)=sign(0.1+sign(real(diagram_out(ii,1))));

% weights adaption by RLS algorithm

    Xin = Xin/scale;
    Yest = W*Xin;
```

```
    Eest = Yin-Yest;

    Z = Xin'*R;
    Q = Z*Xin;
    V = 1/(Rho+Q);
    Zhat = V.*R*Xin;
    R = (1/Rho).*(R-Zhat*Z);
    W = W + Eest*Zhat';

% BER and MSE calculation

    error(ii,1) = diagram_out(ii,1)-ideal_data(ii,1);
    error_real(ii,1) = real(diagram_out(ii,1))-ideal_data(ii,1);

    mse(ii,1) = error(ii,1)*conj(error(ii,1));
    mse_real(ii,1) = error_real(ii,1)*conj(error_real(ii,1));

    if ii>1

       MSE_adj(ii,1) = step*mse(ii,1)+(1-step)*MSE_adj(ii-1,1);
       MSE_real_adj(ii,1) = step*mse_real(ii,1)+(1-step)*MSE_real_adj(ii-1,1);
    end;


    if (final_data(ii,1)~=ideal_data(ii,1))
        train_error=train_error+1;
    end;


 end;  % end of train sequence processing



%                 .....

%                 .          Blind  TDAF Processing          .

%                 .....


    dmin=2;
    perc=0.2;
    Rb2=-(dmin^2)/(4*log(perc));
```

```
    step=1/8;                          % smooth factor

    Sym0 = fft(-ref_code,fft_n);       % reference FFT for data -1
    Sym1 = fft(ref_code,fft_n);        % reference FFT for data +1


  for jj=L_train+1:L


    if (jj-1)/L_part==fix((jj-1)/L_part)

       gen_data;                       % generate data periodically

    end;


    pos=jj-fix((jj-1)/L_part)*L_part;
    k_low=(pos-1)*orders+1;
    k_up =pos*orders;

    input_sample=channel(k_low:k_up,1);
    Xin=fft(input_sample,fft_n);


    Yest=W*Xin;

    d_out(k_low:k_up,1)=ifft(Yest,orders);      % transfer back to time domain
    y_out=d_out(k_low:k_up,1).*ref_code;        % despreading

    diagram_out(jj,1) = sum(y_out)/orders;
    constell_out(jj,1)=diagram_out(jj,1);

%  AGC control

    scale=abs(diagram_out(jj,1))*step+(1-step)*scale;
    diagram_out(jj,1)=diagram_out(jj,1)/scale;


%  weights adaption Exponential_law

    Xin = Xin/scale;
    Yest = W*Xin;
```

```
Err0=Sym0-Yest;
Err1=Sym1-Yest;

T0=(1/orders^2)*(Err0'*Err0);
T1=(1/orders^2)*(Err1'*Err1);


if  T1>=T0

   Eest=Sym0-Yest;
   Psi=exp(-T0/Rb2);

else

   Eest=Sym1-Yest;
   Psi=exp(-T1/Rb2);

end;

Z = Xin'*R;
Q = Z*Xin;
V = 1/(Rho+Q);
Zhat = V.*R*Xin;
R = (1/Rho).*(R-Zhat*Z);
W = W + Psi.* Eest*Zhat';


final_data(jj,1)=sign(0.1+sign(real(diagram_out(jj,1))));

% BER and MSE calculations

error(jj,1)=diagram_out(jj,1)-ideal_data(jj,1);
error_real(jj,1)=real(diagram_out(jj,1))-ideal_data(jj,1);

mse(jj,1)=error(jj,1)*conj(error(jj,1));
mse_real(jj,1)=error_real(jj,1)*conj(error_real(jj,1));

MSE_adj(jj,1)=step*mse(jj,1)+(1-step)*MSE_adj(jj-1,1);
MSE_real_adj(jj,1)=step*mse_real(jj,1)+(1-step)*MSE_real_adj(jj-1,1);


if (final_data(jj,1)~=ideal_data(jj,1))
    blind_error=blind_error+1;
```

```
    end;


  end;  % end of binder equalizer processing


    total_error=train_error+blind_error          % total processing errors
    blind_error                                  % blind processing errors
    BER=blind_error/(L-L_train)                  % BER
    SIR=-10*log10(mean(MSE_real_adj))            % SIR at output


%   writing results to file

    clean_fid = fopen('show.ret','w');
    fclose(clean_fid);
    record_fid = fopen('show.ret','a');
    para = fprintf(record_fid,'\n ----------System Parameters---------\n');
    para = fprintf(record_fid,'\n Co-channel user number is  %d\n',User_N);
    para = fprintf(record_fid,'\n SNR is  %d (dB)\n',SNR);
    para = fprintf(record_fid,'\n Narrow Band FM interference source number is %d\n',FM_n);
    para = fprintf(record_fid,'\n Adjacent channel user number is %d \n',adj_User_N);
    para = fprintf(record_fid,'\n adjacent channel has %d (dB) near-far power
advantage\n',mean(adj_power_dB)*adj_User_N);
    para = fprintf(record_fid,'\n second ray delay is %d sample intervals\n',path2);
    para = fprintf(record_fid,'\n attenation on second ray %d dB\n',power_ray2);
    para = fprintf(record_fid,'\n vehicle speed is %d mph\n',speed_mph);
    para = fprintf(record_fid,'\n Data length for blind equalizer is %d\n',L-L_train);
    para = fprintf(record_fid,'\n Bit Error Rate (BER) is %f\n',BER);
    para = fprintf(record_fid,'\n SIR at output is %f dB\n',SIR);
    fclose(record_fid);

%  ************* end of file 'plain.m' *****************




%   Signals generation control program
%
%   key parameters:
%         User_N          co_channel users
%         adj_User_N      adjacent channel users
%         adj_power_dB    power in adjacent channel
```

```
%          FM_N          FM interference sources
%          FM_amp_dB     FM signal power
%          SNR           signal-to-noise ratio
%          speed_mph     vehicle speed
%          Length        data points number
%



%                  ..........................................................

%                  .          Data generation control          .

%                  ..........................................................



    head =1;
    feet  = L_part*orders;
    LL=feet-head+1;

    lpf_beta =16;
    bb_low=8;
    up_times=2;

%  SOI data generation

    ref_data=sign(0.1-sign(randn(L_part,1)));
    ideal_data(max(ii,jj)+(0:L_part-1),1)=ref_data;

%  spreading for SOI

    load gold_codes.mat;
    ref_code=reshape(ones(orders/chips,1)*gcodes(1:chips,1)',orders,1);
    pureCDMA_sample = reshape(ref_code*ref_data(1:L_part,1)',LL,1);

    sample_factor = orders/chips;
    mixCDMA_sample=zeros(LL,1);


%  multi-access interference for SNOI1

    for ia=1:User_a
```

```
        phase_user_a(1:User_a,1)=2*pi*rand(User_a,1);
        amp_a(1:User_a,1)=1.0*ones(User_a,1);
        code_a=gcodes(1:chips,ia+1);
        user_data_a = sign(0.1+sign(randn(LL/orders,1)));
        block_code_a = reshape(ones(sample_factor,1)*code_a',orders,1);
        sample_a = reshape(block_code_a*user_data_a',LL,1);
        shift = amp_a(ia,1)*cos(phase_user_a(ia,1)+j*sin(phase_user_a(ia,1)));
        mixCDMA_sample = shift*sample_a+mixCDMA_sample;

    end;


% multi-access interference for SNOI2

    for ib=1:User_b

        phase_user_b(1:User_b,1)=2*pi*rand(User_b,1);
        amp_b(1:User_b,1)=1.0*ones(User_b,1);
        code_b = gcodes(1:chips2,ib+User_a);
        user_data_b = sign(0.1+sign(randn(LL/orders2,1)));
        block_code_b = reshape(ones(sample_factor,1)*code_b',orders2,1);
        sample_b = reshape(block_code_b*user_data_b',LL,1);
        shift = amp_b(ib,1)*(cos(phase_user_b(ib,1))+j*sin(phase_user_b(ib,1)));
        mixCDMA_sample = shift*sample_b+mixCDMA_sample;

    end;


% multi-access interference for SNOI3

    for ic=1:User_c

        phase_user_c(1:User_c,1)=2*pi*rand(User_c,1);
        amp_c(1:User_c,1)=1.0*ones(User_c,1);
        code_c = gcodes(1:chips3,User_a+User_b+ic);
        user_data_c = sign(0.1+sign(randn(LL/orders3,1)));
        block_code_c = reshape(ones(sample_factor,1)*code_c',orders3,1);
        sample_c = reshape(block_code_c*user_data_c',LL,1);
%       sample_c =sign(randn(LL,1));
        shift = amp_c(ic,1)*(cos(phase_user_c(ic,1))+j*sin(phase_user_c(ic,1)));
        mixCDMA_sample=shift*sample_c+mixCDMA_sample;

    end;
```

```
% spectral shaping

    baseCDMA_sample = baseCDMA_data.m

% Add noise

    p_noise = 10^(-SNR/10);
    amp_noise = sqrt(p_noise/2);
    noise_sample = amp_noise*(1+j)*randn(LL,1)/sqrt(2);


% narrowband FM interference


    mixFM_data;

% Rayleigh fading

    ray_amp = Rayleigh(maxshift,sample_rate,LL);
    baseCDMA_sample = baseCDMA_sample.*ray_amp;

 if  path2<2

    delay_sample=zeros(LL,1);

 else

    mpath_model = zeros(path2,1);
    mpath_model(path2,1) = -10^(power_ray2/10)/sqrt(2);

    delay_sample = filter(mpath_model,[1],pureCDMA_sample);

    ray_amp2 = Rayleigh(maxshift,sample_rate,LL);
    delay_sample = delay_sample.*ray_amp2;

 end;

% adjacent channel interference

    Sidelobe_data;
```

```
% Summation of all the interference codes
    interfer_sample = mixCDMA_sample+mixFM_sample+delay_sample+sidelobe_sample;
    if var(interfer_sample) > 0
        SIR_input = 10*log(var(interfer_sample));
    else
        SIR_input = 0;
    end;
    channel(head:feet,1) = baseCDMA_sample+noise_sample+interfer_sample;
% receiver spectral shaping
    Receiver_data;

% ********** end of file 'data_gen.m' ************
```

Vita

Raymond Sihao Zheng was born in Shanghai, China on October 21, 1970. He received his Bachelor of Science in Electrical Engineering from Shanghai Jiao Tong University, Shanghai, China in July, 1992. In 1992, he joined the Mobile and Portable Radio Research Group at Virginia Tech. From July, 1993 to Jan, 1994, he worked as an intern in the Network Operations of Cellular ONE/Washington and Baltimore, where he work for microcell and PCS system testing. In MPRG, he focused on the research of channel modeling, system capacity and interference rejection for CDMA Automatic Vehicle Monitoring systems. In November, 1994, he wll to work with Bell Northern Research (BNR)/Richarson, TX as a member of technical staff. His research interest includes channel modeling for digital cellular system, RF performance optimization and mircocell systems development.